
AtmosArena: Benchmarking Foundation Models for Atmospheric Sciences

Anonymous Author(s)

Affiliation

Address

email

Abstract

1 Deep learning has emerged as a powerful tool for atmospheric sciences, showing
2 significant utility across various tasks in weather and climate modeling. In line with
3 recent progress in language and vision foundation models, there are growing efforts
4 to scale and finetune such models for multi-task spatiotemporal reasoning. Despite
5 promising results, existing works often evaluate their model on a small set of non-
6 uniform tasks, which makes it hard to quantify broad generalization across diverse
7 tasks and domains. To address this challenge, we introduce AtmosArena, the first
8 multi-task benchmark dedicated to foundation models in atmospheric sciences.
9 AtmosArena comprises a suite of tasks that cover a broad spectrum of applications
10 in atmospheric physics and atmospheric chemistry. To showcase the capabilities
11 and key features of our benchmark, we conducted extensive experiments to evaluate
12 two state-of-the-art deep learning models, ClimaX and Stormer on AtmosArena,
13 and compare their performance with other deep learning and traditional baselines.
14 By providing a standardized, open-source benchmark, we aim to facilitate further
15 advancements in the field, much like open-source benchmarks have driven the
16 development of foundation models for language and vision.

17 1 Introduction

18 Modeling of large-scale atmospheric systems is an omnipresent challenge for science and society.
19 Traditionally, numerical methods are the dominating approach in atmospheric sciences, which
20 operationalize rigorous systems of differential equations to simulate such phenomena [50, 10].
21 Despite their widespread use in practice, numerical methods suffer from many challenges, such as
22 inadequate resolution of important small-scale physical processes and substantial computational
23 demands [9, 45, 46, 77]. Deep learning has emerged as a powerful complement due to its ability to
24 learn complex systems from historical data and produce fast predictions within seconds. Deep learning
25 methods have proven great utility and performance across various atmospheric tasks, including but
26 not limited to precipitation nowcasting [79, 87, 4], medium-range weather forecasting [101, 73, 38,
27 64, 13, 44, 61, 20, 19, 41], climate projection [98], climate downscaling [7, 48, 56, 81, 84, 91], air
28 pollution forecasting [6, 11, 90, 16, 35], and greenhouse gas emission prediction [31, 8, 3].

29 Recent years have witnessed a paradigm shift from training task-specific models to developing
30 foundation models for atmospheric sciences [59, 14], similar to models such as GPT-x [15, 1] in
31 natural language processing, or CLIP [71] in computer vision. These foundation models are trained
32 on large-scale and diverse datasets, enabling them to develop a rich, general understanding of the
33 atmosphere. Once pre-trained, they can adapt efficiently to various downstream tasks, ranging from
34 weather nowcasting to long-term climate projections, via lightweight finetuning. This approach is
35 particularly attractive for atmospheric sciences, where there is an increasing availability of high-
36 quality datasets and tasks have non-trivial global and regional structure.

Table 1: Comparisons between AtmosArena and existing works that consider multiple atmospheric tasks. AtmosArena offers the most comprehensive set of tasks, data, and evaluation metrics.

Benchmark	Tasks	Data	Metrics
AtmosArena	Weather forecasting	ERA5	RMSE, ACC
	S2S forecasting	ERA5	RMSE, ACC, Spectral Div
	Climate data infilling	ERA5, Berkeley Earth	Bias, RMSE
	Climate model emulation	ClimateBench	Spatial, Global, Total, RMSE
	Climate downscaling	ERA5	RMSE, Bias, Pearson
	Extreme weather events detection	ClimateNet	IoU, Precision, Recall, F-1
ClimateLearn	Weather forecasting	ERA5	RMSE, ACC
	Downscaling	ERA5	RMSE, Bias, Pearson
	Projection	ClimateBench	Spatial, Global, Total, RMSE
ClimaX	Weather forecasting	ERA5	RMSE, ACC
	S2S forecasting	ERA5	RMSE, ACC
	Climate model emulation	ClimateBench	Spatial, Global, Total, RMSE
	Climate downscaling	ERA5	RMSE, Bias, Pearson
Aurora	Weather forecasting	HRES Analysis	RMSE, ACC
	Air composition forecasting	CAMS Analysis	RMSE, ACC

Standardized open-source benchmarks are crucial for the advancement of foundation models. In language, benchmarks such as HeLM [47], LLM Foundry, LM Evaluation Harness [26], and Big Bench [88] have aided researchers to systematically evaluate the performance of large language models. Similarly, for perception, comprehensive benchmarks such as VQA [5], SciBench [96], MMMU [105], and MathVista [49], have significantly accelerated research in multimodal foundation models. In stark contrast, there is no standardized multi-task benchmark for benchmarking atmospheric foundation models and existing works [59, 14] limit their evaluation to a relatively small set of non-overlapping tasks, which creates challenges in objective assessment of progress in the field.

To address this gap, we introduce AtmosArena, an open-source benchmark for foundation models in atmospheric sciences. To the best of our knowledge, AtmosArena is the first of its kind to offer a comprehensive evaluation framework tailored for this domain. AtmosArena encompasses a suite of tasks that span a wide spectrum of problems from both atmospheric and machine learning perspectives. Each task within AtmosArena is supported by datasets, fine-tuning protocols, evaluation code, standardized evaluation metrics, and a collection of deep learning and traditional baselines. This suite not only facilitates a fair assessment of model performance but also serves as a crucial tool for identifying opportunities for future development in the field. AtmosArena aims to set a new standard in the evaluation of atmospheric models, providing a solid foundation for the development of new methodologies. Table 1 summarizes the tasks, datasets, and metrics supported by AtmosArena.

To showcase the utility of AtmosArena, we conduct extensive experiments across all tasks included in the benchmark. We test and compare three representative classes of models: (1) deep learning with no pretraining, (2) single-source pretraining, and (3) multi-source pretraining. We also include traditional methods as simple baselines. To ensure fairness, we maintained consistent fine-tuning and evaluation settings across all models. The experimental results indicate that pretrained models generally outperform baselines without pretraining in most tasks. However, no single model consistently dominates across all tasks. This underscores the comprehensiveness of AtmosArena and highlights potential opportunities for future model development. In line with our commitment to openness and reproducibility, we will make all our data, code, and model checkpoints publicly available.

2 Related Work

Deep Learning for Atmospheric Sciences Deep learning has revolutionized atmospheric sciences in recent years in both speed and accuracy. In weather forecasting, notable models like Pangu [13], Graphcast [44], and Stormer [61] have surpassed the accuracy of the gold-standard IFS HRES system. This progress spans from simple models like ResNet [73] to advanced architectures such as Graph Neural Networks [38, 44], Fourier neural operators [63], and Transformers [13, 59, 21, 19, 61]. In addition to medium-range, other works focus on forecasting at different time scales, such as nowcasting [87, 78, 4] or longer-term prediction tasks [99, 54]. To account for uncertainty, recent

72 works have also proposed ensemble forecasting with hybrid-physics models [42] or diffusion [68],
73 which are particularly useful for extreme event prediction like heavy rainfall [106] and floods [58].

74 **Foundation Models for Atmospheric Sciences** ClimaX [59] is the first foundation model for
75 weather and climate, pretrained on five simulated datasets from CMIP6 and finetuned on four
76 downstream tasks. Aurora [14] is the latest atmospheric foundation model which scaled up pretraining
77 to larger models, more data, and finer grid resolutions. Aurora was shown to achieve state-of-the-
78 art performance in operational weather forecasting and air composition forecasting. In addition
79 to atmospheric sciences, the development of scientific foundation models for physical domains is
80 growing quickly as a field. For example, recent works in Partial Differential Equations (PDEs)
81 modeling have proposed to pretrain large-scale models for micro-scale dynamical systems that can
82 transfer in a zero-shot or few-shot fashion to unseen equations [89, 33, 2, 52].

83 **Atmospheric Datasets and Benchmarks** Standardized benchmarks fuel the growth of atmo-
84 spheric deep learning. WeatherBench [74, 76] provides data, metrics, baselines, and a leaderboard
85 for medium-range weather forecasting. Another common data source for weather forecasting is
86 CMIP6 [24] which provides a large collection of simulation runs from climate models. Subseasonal-
87 ClimateUSA [55] and ChaosBench [57] are two recent benchmarks that have been proposed to push
88 the forecasting capabilities to sub-seasonal and seasonal time scales. Beyond forecasting, standard
89 datasets have been developed for a diverse set of tasks in weather and climate, including climate emu-
90 lation [37], sub-resolution physics modeling [104], precipitation prediction [22, 86], extreme weather
91 events detection and localization [72, 80, 53, 67, 70], natural disaster-related tasks [69], atmospheric
92 radiative transfer [17], long-term global trends prediction [98], cloud classification [75], nowcast-
93 ing [25], tropical cyclone intensity prediction [51], air quality metrics prediction [12], hydrometeoro-
94 logical time series analysis [93], and river flow analysis [28]. Beyond plain datasets, libraries such
95 as ClimateLearn [60], Scikit-downscale [30], CCdownscaling [65], and CMIP6-Downscaling [18]
96 provide software for training deep learning methods for various tasks in atmospheric sciences.

97 3 Key Components of AtmosArena

98 As a first benchmark, we aim to build a comprehensive suite of tasks in atmospheric sciences,
99 emphasizing diversity from both domain-specific and machine learning perspectives. Domain-wise,
100 tasks are broadly classified into atmospheric physics or atmospheric chemistry. Atmospheric physics
101 focuses on physical variables like temperature, humidity, and wind, essential for modeling weather
102 patterns in the short-term and climate trends in the longer term. Atmospheric chemistry, on the other
103 hand, focuses on the composition and transformation of atmospheric constituents, such as pollutants
104 like carbon monoxide and dioxide, crucial for studying air quality and environmental health.

105 Due to space constraints, this section presents the six tasks under atmospheric physics: Medium-range
106 Weather Forecasting, S2S Forecasting, Extreme Weather Events Detection, Climate Downscaling,
107 Climate Data Infilling, and Climate Model Emulation. Tasks related to atmospheric chemistry are
108 detailed in Appendix F. From a machine learning perspective, many common predictive tasks in
109 atmospheric sciences can be mapped to well-defined problems in machine learning. Within this
110 perspective, our benchmark can be seen as spanning five distinct categories of tasks defined on a grid:
111 forecasting, segmentation, super-resolution, inpainting, and counterfactual prediction. This diverse
112 suite of tasks allows us to obtain a holistic evaluation of atmospheric foundation models.

113 3.1 Tasks

114 **Medium-range weather forecasting** is the task of predicting the global weather conditions at a
115 future time step $t + T$ given the weather conditions at or before the current step t , where the lead time
116 T ranges from a few hours to two weeks. A deep learning model takes an input of shape $V \times H \times W$
117 and outputs a prediction of shape $V' \times H \times W$, in which V and V' are the numbers of input and
118 output atmospheric variables, respectively, while $H \times W$ denotes the spatial resolution of the data.

119 **Sub-seasonal-to-seasonal (S2S) forecasting** is similar to medium-range forecasting but with a longer
120 lead time range between 2 weeks and 2 months [95, 94]. This task bridges the gap between weather
121 forecasting and climate modeling and holds significant socioeconomic value in disaster mitigation,
122 but has received much less attention than the other two well-established tasks. Since the weather

123 becomes too chaotic for any model to perform accurate point prediction after two weeks, we instead
124 task the models to forecast the average statistics of key variables over a two-week window.

125 **Extreme weather events detection** is the task of identifying weather patterns that may lead to
126 extreme weather events, such as tropical cyclones and atmospheric rivers. Deep learning models are
127 trained to perform pixel-level detection and segmentation of these events in climate data. Specifically,
128 the input typically consists of key atmospheric variables, and the output is a segmented map where
129 each pixel is classified as part of an extreme event or as background. This approach allows for precise
130 quantification of the frequency, intensity, and spatial extent of extreme events under various climate
131 scenarios, providing valuable insights for climate research and policy-making.

132 **Climate downscaling** is the task of improving the spatial resolution of climate model outputs, which
133 typically operate on large grid cells due to their high computational demands. This refinement is
134 crucial for accurately representing local phenomena and informing regional policy decisions. In this
135 task, deep learning models transform an input grid of dimensions $V \times H \times W$ into a higher-resolution
136 output $V' \times H' \times W'$, where $H' > H$ and $W' > W$.

137 **Climate data infilling** involves estimating missing or incomplete data in historical and current
138 climate datasets. This task aims to provide a more comprehensive and continuous historical record
139 of important atmospheric variables, such as near-surface air temperature, enabling robust climate
140 analysis and modeling. In data infilling, deep learning models are trained to predict missing values
141 by leveraging patterns found in available data. The typical input to these models includes incomplete
142 datasets of dimensions $V \times H \times W$, and the output is a complete dataset of the same dimensions,
143 where the previously missing values are estimated by the model.

144 **Climate model emulation** involves predicting the annual mean global distributions of crucial climate
145 variables like surface temperature and precipitation indices, given different scenarios of anthropogenic
146 forcing factors such as carbon dioxide (CO_2) and methane (CH_4). The input is a tensor of shape
147 $T \times V \times H \times W$ which captures the forcing conditions over T consecutive years, and the output
148 shape is $V' \times H \times W$. Unlike temporal forecasting, this task assesses a model’s ability to predict
149 the response of the climate system to varying levels of external factors, providing a foundation for
150 long-term climate strategy and policy decisions.

151 3.2 Datasets

152 **ERA5** maintained by ECMWF [34] is a common dataset for training and evaluating data-driven
153 methods in atmospheric sciences [13, 44, 61]. ERA5 is a reanalysis dataset that provides the best
154 guess of different climate variables at any point in time by integrating observational data with an
155 advanced forecasting model known as the Integrated Forecasting System (IFS) [100]. ERA5 offers
156 hourly data from 1979 to the present and at a 0.25° (721×1440) global grid, totaling nearly 400,000
157 data points at 37 different pressure levels and the Earth’s surface. Given its extensive scale, we regrid
158 the original data to 1.40625° (128×256) grid and consider data from 1979 to 2020 for training
159 and evaluation. We use ERA5 for four tasks in AtmosArena, including medium-range weather
160 forecasting, S2S forecasting, climate downscaling, and data infilling.

161 **Berkeley Earth** provides a variety of high-quality temperature data products that incorporate a large
162 set of temperature observations [82]. In AtmosArena, we use the global monthly average temperature
163 data at 1° (180×360) grid as an independent test dataset for the infilling task. We regrid the data to
164 the common resolution of 1.40625° .

165 **ClimateBench** is a benchmark for testing data-driven methods for climate model emulation [98].
166 ClimateBench consists of simulation outputs of the Norwegian Earth System Model (NorESM2) [85]
167 from CMIP6 [23] that are run under different forcing scenarios for the period 2015 – 2100. The
168 dataset includes four input forcing factors – carbon dioxide (CO_2), sulfur dioxide (SO_2), black carbon
169 (BC), and methane (CH_4), and the annual mean global distributions of four target variables – surface
170 temperature, diurnal temperature range, precipitation, and the 90th percentile of precipitation.

171 **ClimateNet** is an expert-labeled dataset of tropical cyclones (TCs) and atmospheric rivers (ARs), two
172 important weather patterns that may lead to extreme weather events [66]. ClimateNet consists of 459
173 time steps (data points) of simulation runs of the Community Atmospheric Model (CAM5.1) from
174 1996 – 2013. Each data point has a spatial resolution of 768×1152 with a total of 16 atmospheric
175 variables, and each pixel is labeled with one of three classes – TCs, ARs, and Background.

176 3.3 Models

177 We consider a state-of-the-art representative from three classes of models. Many other recent models
178 would also benefit from this benchmark [14, 68], but they are currently closed-source. Over time, we
179 plan to maintain a public leaderboard to allow for evaluation of both open and closed source models.

180 **Non-pretrained model** We aim to provide state-of-the-art methods tailored to each specific task in
181 AtmosArena. For tasks where there is no established baseline, we use UNet [83] as the deep learning
182 baseline. We chose UNet due to its excellent performance in a variety of dense prediction tasks
183 in computer vision, which resemble most of the atmospheric tasks included in AtmosArena. The
184 Unet models we train in the experiments have the same size of 500M parameters, for which we have
185 performed extensive hyperparameters tuning to obtain a strong non-pretrained baseline.

186 **Single-source pretrained model** We include Stormer [61], a state-of-the-art open-source deep learn-
187 ing model for medium-range weather forecasting. Stormer is a transformers-based architecture [92]
188 that was trained on 6-hourly ERA5 data at 1.40625° resolution from 1979 to 2018. We chose Stormer
189 since it was trained on the same spatial resolution as our datasets, and its simple architecture allows
190 seamless finetuning on new tasks. Stormer has 400M parameters.

191 **Multi-source pretrained model** We include ClimaX [59], the first large-scale atmospheric founda-
192 tion model trained on multiple data sources. ClimaX was pretrained to perform temporal forecasting
193 on five simulated datasets at 1.40625° from CMIP6 [23] and was shown to transfer well to various
194 atmospheric tasks via finetuning. Since ClimaX and Stormer share similar transformer architectures
195 and training objectives, comparing them helps examine if and when multi-source pretraining is
196 beneficial to the model. ClimaX has 100M parameters.

197 3.4 Finetuning protocols

198 ClimaX and Stormer share a similar architecture, which consists of an embedding layer, a transformer
199 backbone, and a prediction head. The embedding layer transforms an input of shape $V \times H \times W$
200 to a sequence of shape $(H/p \times W/p) \times D$, where $(H/p \times W/p)$ is the sequence length, p is the
201 patch size, and D is the hidden dimension. The transformer backbone processes this sequence and
202 outputs a sequence of the same shape, and finally the prediction head outputs a prediction of shape
203 $V' \times H' \times W'$. We refer to the original papers for a detailed description of these models.

204 We consider two finetuning settings, one where we freeze the core transformer backbone, and the other
205 where we finetune the entire network. The frozen setting helps examine the direct transferability of the
206 pretrained backbone to new tasks without further training. In tasks where the input or target variables
207 were unseen during pretraining, we replace the pretrained embedding layer and prediction head with
208 newly initialized networks. For datasets having a different spatial resolution from pretraining data,
209 we interpolate the pretrained positional embedding to match the new sequence length.

210 4 Benchmark Evaluation

211 This section evaluates different models on six atmospheric physics tasks described in Section 3.1.
212 Through the experiments, we aim to showcase the breadth of AtmosArena and provide practical rec-
213 ommendations for finetuning atmospheric foundation models on new tasks. We refer to Appendix G
214 for the atmospheric chemistry experiments. We also present infilling results on the Berkeley Earth
215 dataset and regional case studies on S2S forecasting in Appendix G.

216 4.1 Medium-range weather forecasting

217 We compare ClimaX and Stormer with Graphcast [44] – a leading forecasting method, and Clima-
218 tology – a simple baseline, on weather forecasting with lead times from 1 to 14 days. We consider
219 six target variables: temperature at 2 meters (T2m), zonal (U10m) and meridional (V10m) wind
220 at 10 meters, geopotential at 500hPa (Z500), temperature at 850hPa (T850), and specific humidity
221 at 700hPa (Q700), which are commonly used to verify forecasting models in previous works.
222 Since Stormer and Graphcast were trained specifically for forecasting, we roll-out the pretrained
223 checkpoints to obtain forecasts at different lead times without further training. For ClimaX, we
224 perform full finetuning for each specific lead time and target variable, following the protocol in the

225 original paper. All deep learning methods are trained on ERA5 from 1979 to 2018 and tested on
 226 2020. The same data split is used for other tasks unless noted otherwise.

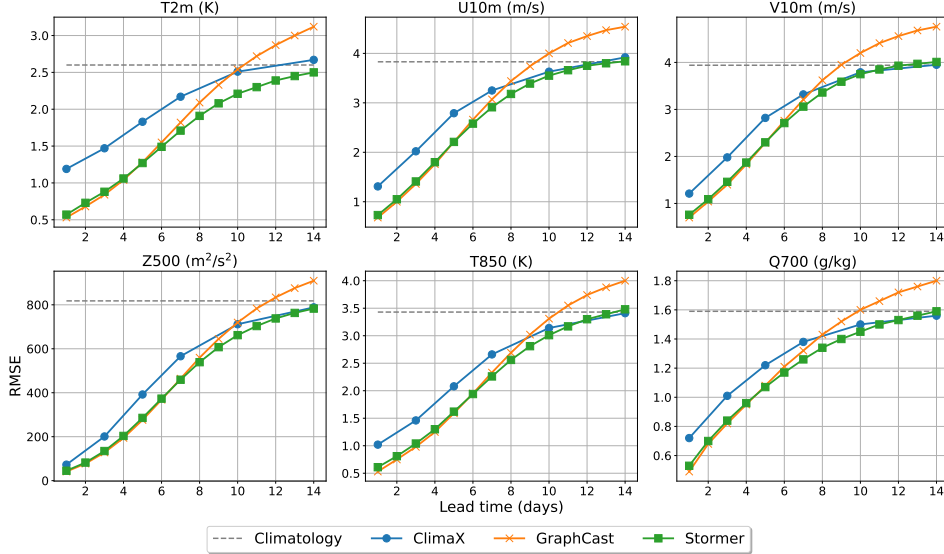


Figure 1: Medium-range weather forecasting performance measured by RMSE on six key variables at different lead times. Solid lines are deep learning models and the dashed line denotes the climatology baseline. Lower RMSE indicates better performance.

227 Figure 1 summarizes the RMSE results of this task (see Appendix for other metrics). Stormer is the
 228 best overall method, performing competitively with Graphcast at short lead times and much better at
 229 longer time scales. Graphcast works well for short lead times, but its performance degrades quickly
 230 and becomes worse than Climatology after day 10. Climax, on the other hand, performs poorly at
 231 small lead times but surpasses Graphcast at around day 10 and catches Stormer at day 14. This is
 232 because Climax performs direct forecasting which avoids error accumulation at long lead times.

233 4.2 Subseasonal-to-seasonal (S2S) forecasting

234 We evaluate Climax, Stormer, and Unet on forecasting the biweekly average statistics of four target
 235 variables – Z500, T850, T2m, and Q700. We consider two lead times of 2 weeks and 4 weeks, in
 236 which the average statistics are computed over weeks 3-4 and weeks 5-6, respectively. We construct
 237 the biweekly average data for training and evaluation from ERA5. For each baseline, we train two
 238 separate models to predict directly the average values at two different lead times. For Climax and
 239 Stormer, we consider two finetuning protocols where we either freeze (Climax frozen and Stormer
 240 frozen) or finetune (Climax finetuned and Stormer finetuned) the transformer backbone. Similar
 241 to medium-range weather forecasting, we include Climatology to examine if deep learning models
 242 achieve meaningful skills for S2S forecasting compared to this simple baseline.

Table 2: S2S performance measured by RMSE and ACC on four target variables at two lead times.

		Z500		T850		T2m		Q700	
		Weeks 3-4	Weeks 5-6	Weeks 3-4	Weeks 5-6	Weeks 3-4	Weeks 5-6	Weeks 3-4	Weeks 5-6
RMSE (↓)	Climax frozen	458.53	471.58	1.79	1.84	1.67	1.73	0.69	0.70
	Climax finetuned	453.05	469.92	1.77	1.80	1.65	1.70	0.69	0.71
	Stormer frozen	461.19	467.37	1.77	1.81	1.56	1.69	0.70	0.72
	Stormer finetuned	466.82	475.06	1.79	1.84	1.64	1.75	0.71	0.72
	Unet	498.46	521.32	1.90	2.09	1.63	2.29	0.74	0.75
	Climatology	475.58	475.58	2.00	2.00	1.61	1.61	0.76	0.76
ACC (↑)	Climax frozen	0.84	0.81	0.92	0.90	0.96	0.95	0.86	0.84
	Climax finetuned	0.84	0.81	0.92	0.90	0.95	0.94	0.86	0.84
	Stormer frozen	0.78	0.77	0.88	0.87	0.95	0.94	0.81	0.81
	Stormer finetuned	0.77	0.77	0.87	0.87	0.94	0.93	0.82	0.82
	Unet	0.84	0.84	0.92	0.91	0.97	0.93	0.85	0.85
	Climatology								

243 Table 2 summarizes the results of S2S forecasting. In terms of RMSE, both ClimaX and Stormer
 244 have meaningful skills except for T2m, while Unet underperforms Climatology for most variables.
 245 Interestingly, the frozen version of ClimaX and Stormer performs competitively to their fully finetuned
 246 counterpart. This result highlights the importance of pretraining, which allows models to efficiently
 247 transfer to new forecasting tasks without further training of the transformer backbone. In terms of
 248 ACC, ClimaX and Unet perform similarly while Stormer lags behind. Overall, ClimaX outperforms
 249 Stormer in this task despite having a poorer performance on medium-range weather forecasting.
 250 This can be explained by the difference between the pretraining objective of the two models, where
 251 ClimaX was trained to perform forecasting at much longer horizons (6 hours to 1 week) compared to
 252 Stormer (6 hours to 1 day).

253 4.3 Climate downscaling

254 We consider the task of downscaling for six key variables: Z500, T850, T2m, Q700, U10m, and V10m.
 255 We use ERA5 at 5.625° as the low-resolution input, and ERA5 at 1.40625° as the high-resolution
 256 target, corresponding to $4\times$ upsampling. We include Unet as a deep learning baseline in addition
 257 to the two finetuning versions of ClimaX and Stormer. We report RMSE and Absolute Mean Bias,
 258 which is the absolute difference between the spatial mean of predictions and ground-truths.

Table 3: Downscaling performance measured by RMSE and Absolute Mean Bias on six variables.

		Z500	T850	T2m	Q700	U10m	V10m
RMSE (\downarrow)	ClimaX frozen	105.49	0.93	1.16	0.70	1.02	1.01
	ClimaX finetuned	74.62	0.78	0.94	0.61	0.83	0.83
	Stormer frozen	104.26	0.95	1.12	0.76	1.07	1.05
	Stormer finetuned	38.84	0.57	0.62	0.55	0.64	0.64
	Unet	47.65	0.66	0.73	0.56	0.70	0.70
Absolute Mean Bias (\downarrow)	ClimaX frozen	28.660	0.167	0.054	0.001	0.032	0.009
	ClimaX finetuned	13.830	0.153	0.119	0.002	0.007	0.001
	Stormer frozen	17.540	0.046	0.048	0.001	0.019	0.011
	Stormer finetuned	0.090	0.051	0.031	0.001	0.011	0.017
	Unet	8.790	0.140	0.040	0.005	0.011	0.006

259 Table 3 shows the performance of the considered methods. Unlike the forecasting tasks, there is
 260 a significant gap between the frozen and the fully finetuned models of ClimaX and Stormer. This
 261 indicates that the transformer backbone pretrained for temporal forecasting might be sub-optimal
 262 for spatial downscaling and further finetuning is required to achieve good performance. Stormer
 263 is the best model in this task with the lowest RMSE and Absolute Mean Bias for most variables,
 264 followed by the Unet baseline. Since ClimaX has the lowest parameter count, we hypothesize that
 265 larger models tend to perform better in this task. This observation was also suggested by the scaling
 266 analysis in the original ClimaX paper.

267 4.4 Data infilling

268 We test the ability of foundation models to fill in missing temperature data, which is a common issue
 269 due to gaps in the coverage of observation stations. We construct training and validation data for this
 270 task from ERA5. During training, we generate a random mask for each training data point, with the
 271 mask ratio (missing ratio) drawn from a uniform distribution $r \sim \mathcal{U}[0.1, 0.9]$. We test each model to
 272 perform infilling with a set of mask ratios $r \in \{0.1, 0.3, 0.5, 0.7, 0.9\}$, where a fixed set of masks for
 273 each ratio is pre-generated and saved to disk to maintain evaluation consistency across models.

274 Figure 2 shows the performance of the considered models for different mask ratios. Similar to
 275 downscaling, fully finetuned models work much better than frozen counterparts, and Stormer is the
 276 best method for this task. This result again highlights the difference between temporal and spatial
 277 tasks and the need for full finetuning to achieve good performance.

278 4.5 Climate model emulation

279 We aim to predict the annual mean global distributions of four target variables: surface air temperature,
 280 diurnal temperature range (difference between daily maximum and minimum surface air temperature),
 281 precipitation, and the 90th percentile precipitation. The input variables are four forcing factors:
 282 carbon dioxide (CO_2), sulfur dioxide (SO_2), black carbon (BC), and methane (CH_4). Following

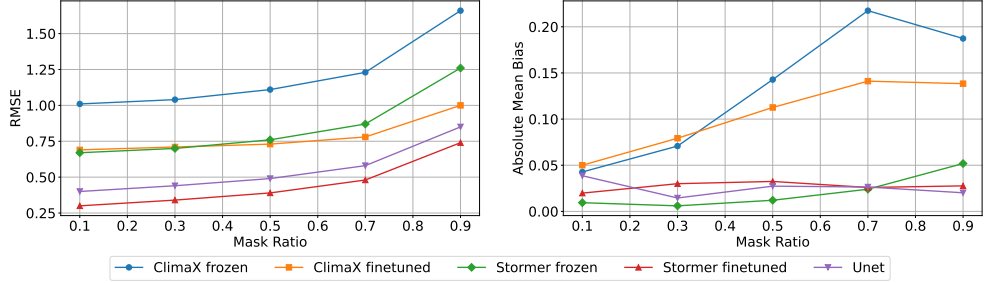


Figure 2: Infilling performance for surface temperature measured by RMSE and Absolute Mean Bias with different missing ratios.

283 ClimateBench, we report NRMSE_s , NRMSE_g , and $\text{NRMSE}_t = \text{NRMSE}_s + 5 \times \text{NRMSE}_g$ as the
 284 evaluation metrics. We use the best method in ClimateBench, namely ClimateBench-NN, as the
 285 baseline in addition to ClimaX and Stormer. We note that in this task, both the input and target
 286 variables were unseen during the pretraining of ClimaX and Stormer, so we replaced their embedding
 287 layer and prediction head with randomly initialized networks. Therefore, the transformer backbone
 288 essentially serves as a feature extractor. We finetune a separate model for each target variable.

Table 4: Climate model emulation performance measured by NRMSE_s , NRMSE_g , and NRMSE_t .

	Surface air temperature			Diurnal temperature range			Precipitation			90th percentile precipitation		
	NRMSE_s	NRMSE_g	NRMSE_t	NRMSE_s	NRMSE_g	NRMSE_t	NRMSE_s	NRMSE_g	NRMSE_t	NRMSE_s	NRMSE_g	NRMSE_t
ClimaX frozen	0.085	0.043	0.297	6.688	0.810	10.739	2.193	0.183	3.110	2.681	0.342	4.389
ClimaX finetuned	0.086	0.043	0.300	7.148	0.961	11.952	2.360	0.206	3.390	2.739	0.332	4.397
Stormer frozen	0.117	0.043	0.334	9.123	0.980	14.022	6.159	0.210	7.211	6.773	0.296	8.254
Stormer finetuned	0.126	0.047	0.361	8.598	0.834	12.767	6.180	0.391	8.136	6.797	0.316	8.376
ClimateBench-NN	0.123	0.080	0.524	7.465	1.233	13.632	2.349	0.151	3.104	3.108	0.282	4.517

289 Table 4 shows the superior performance of ClimaX in this task, outperforming Stormer and the
 290 ClimateBench-NN baseline by a large margin. This result highlights a unique benefit of multi-source
 291 pretraining in acquiring a general-purpose backbone that allows for easy transferability to downstream
 292 tasks and datasets significantly different from pretraining. Moreover, frozen models generally work
 293 better than the fully finetuned counterparts for this task. This can be explained by the small data size
 294 of ClimateBench (754 data points), so further finetuning of the backbone can lead to overfitting and
 295 hurt the test performance. A similar result was observed in the ClimaX paper.

296 4.6 Extreme weather detection

297 Finally, we consider the task of detecting Tropical Cyclones (TCs) and Atmospheric Rivers (ARs),
 298 two atmospheric phenomena highly correlated with extreme weather events. We use the ClimateNet
 299 dataset for finetuning and evaluation, in which we use data from 1996 to 2010 for training and
 300 validation, and 2011 to 2013 for testing. We finetune ClimaX and Stormer to classify each pixel into
 301 one of three classes: TC, AR, and Background (BG). Similar to climate model emulation, we replace
 302 the pretrained embedding and prediction layer with randomly initialized networks. Since ClimateNet
 303 data is of much higher resolution, we increase the patch size to 8 for both ClimaX and Stormer, and
 304 interpolate the pretrained positional embedding to match the new sequence length.

305 Figure 3 compares the performance of ClimaX and Stormer with CGNet [103], a lightweight
 306 segmentation architecture based on CNN specifically designed for this task. Since the BG class
 307 dominates other classes, we adopt the weighted Jaccard loss function [43] to counter this class
 308 imbalance. The two finetuned versions of ClimaX work best in this task with respect to IoU and
 309 F-1, significantly outperforming its counterpart Stormer. This again demonstrates the importance
 310 of multi-source pretraining in obtaining higher transferable backbones. ClimaX also outperforms
 311 CGNet in 3/4 metrics, showing the benefit of foundation models over specialized architectures.

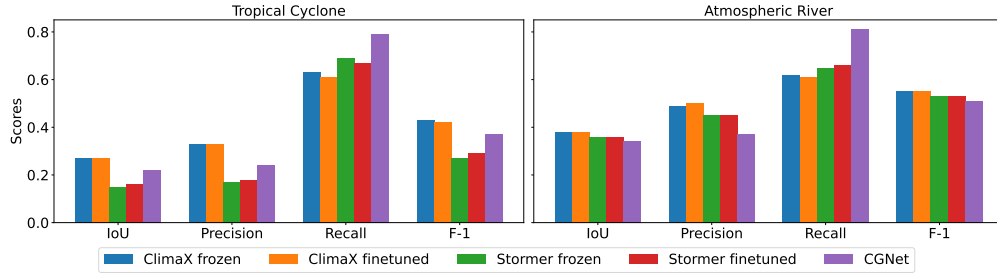


Figure 3: Extreme weather detection performance measured by IoU, Precision, Recall, and F-1.

312 5 Conclusion

313 We presented AtmosArena, the first benchmark dedicated to foundation models in atmospheric
 314 sciences. AtmosArena offers a diverse suite of tasks, datasets, and evaluation metrics to evaluate a
 315 foundation model holistically. AtmosArena not only provides a standard benchmark for comparing
 316 model performance but also serves as a crucial tool for identifying future research works. In
 317 addition, we release all our data, code, and model checkpoints, facilitating reproducible research and
 318 broadening collaborations. Given the vast development of scientific foundation models, we believe
 319 our contribution is timely and useful for both machine learning and atmospheric communities.

320 **Limitations and Future Work** With academic resource constraints, we acknowledge that there are
 321 various directions to improve AtmosArena in each of four dimensions – datasets, tasks, models, and
 322 evaluations. One such direction involves integrating regional datasets and expanding the collection of
 323 supported data sources. On the task side, we plan to include probabilistic tasks that are an important
 324 aspect of modeling weather and climate. For models and evaluations, we plan to find platforms for
 325 hosting atmospheric foundation models, along with an accompanying leaderboard.

326 References

- 327 [1] Josh Achiam, Steven Adler, Sandhini Agarwal, Lama Ahmad, Ilge Akkaya, Florencia Leoni
328 Aleman, Diogo Almeida, Janko Altschmidt, Sam Altman, Shyamal Anadkat, et al. Gpt-4
329 technical report. *arXiv preprint arXiv:2303.08774*, 2023.
- 330 [2] Benedikt Alkin, Andreas Fürst, Simon Schmid, Lukas Gruber, Markus Holzleitner, and
331 Johannes Brandstetter. Universal physics transformers. *arXiv preprint arXiv:2402.12365*,
332 2024.
- 333 [3] S Altikat. Prediction of co2 emission from greenhouse to atmosphere with artificial neural
334 networks and deep learning neural networks. *International Journal of Environmental Science
335 and Technology*, 18(10):3169–3178, 2021.
- 336 [4] Marcin Andrychowicz, Lasse Espeholt, Di Li, Samier Merchant, Alex Merose, Fred Zyda,
337 Shreya Agrawal, and Nal Kalchbrenner. Deep learning for day forecasts from sparse observa-
338 tions. *arXiv preprint arXiv:2306.06079*, 2023.
- 339 [5] Stanislaw Antol, Aishwarya Agrawal, Jiasen Lu, Margaret Mitchell, Dhruv Batra, C Lawrence
340 Zitnick, and Devi Parikh. Vqa: Visual question answering. In *Proceedings of the IEEE
341 international conference on computer vision*, pages 2425–2433, 2015.
- 342 [6] Yasin Akin Ayturan, Zeynep Cansu Ayturan, and Hüseyin Oktay Altun. Air pollution mod-
343 elling with deep learning: a review. *International Journal of Environmental Pollution and
344 Environmental Modelling*, 1(3):58–62, 2018.
- 345 [7] J. Baño Medina, R. Manzananas, and J. M. Gutiérrez. Configuration and intercomparison of
346 deep learning neural models for statistical downscaling. *Geoscientific Model Development*, 13
347 (4):2109–2124, 2020. doi: 10.5194/gmd-13-2109-2020. URL [https://gmd.copernicus.
348 org/articles/13/2109/2020/](https://gmd.copernicus.org/articles/13/2109/2020/).
- 349 [8] Melahat Sevgül Bakay and Ümit Ağbulut. Electricity production based forecasting of green-
350 house gas emissions in turkey with deep learning, support vector machine and artificial neural
351 network algorithms. *Journal of Cleaner Production*, 285:125324, 2021.
- 352 [9] V. Balaji, E. Maisonnave, N. Zadeh, B. N. Lawrence, J. Biercamp, U. Fladrich, G. Aloisio,
353 R. Benson, A. Caubel, J. Durachta, M.-A. Foujols, G. Lister, S. Mocavero, S. Underwood,
354 and G. Wright. CPMIP: measurements of real computational performance of Earth system
355 models in CMIP6. *Geoscientific Model Development*, 10(1):19–34, 2017. doi: 10.5194/
356 gmd-10-19-2017. URL <https://gmd.copernicus.org/articles/10/19/2017/>.
- 357 [10] Peter Bauer, Alan Thorpe, and Gilbert Brunet. The quiet revolution of numerical weather
358 prediction. *Nature*, 525(7567):47–55, 2015.
- 359 [11] Abdellatif Bekkar, Badr Hssina, Samira Douzi, and Khadija Douzi. Air-pollution prediction in
360 smart city, deep learning approach. *Journal of big Data*, 8:1–21, 2021.
- 361 [12] C. Betancourt, T. Stomberg, R. Roscher, M. G. Schultz, and S. Stadtler. Aq-bench: a benchmark
362 dataset for machine learning on global air quality metrics. *Earth System Science Data*, 13
363 (6):3013–3033, 2021. doi: 10.5194/essd-13-3013-2021. URL [https://essd.copernicus.
364 org/articles/13/3013/2021/](https://essd.copernicus.org/articles/13/3013/2021/).
- 365 [13] Kaifeng Bi, Lingxi Xie, Hengheng Zhang, Xin Chen, Xiaotao Gu, and Qi Tian. Pangu-weather:
366 A 3d high-resolution model for fast and accurate global weather forecast. *arXiv preprint
367 arXiv:2211.02556*, 2022.
- 368 [14] Cristian Bodnar, Wessel P Bruinsma, Ana Lucic, Megan Stanley, Johannes Brandstetter,
369 Patrick Garvan, Maik Riechert, Jonathan Weyn, Haiyu Dong, Anna Vaughan, et al. Aurora: A
370 foundation model of the atmosphere. *arXiv preprint arXiv:2405.13063*, 2024.
- 371 [15] Tom Brown, Benjamin Mann, Nick Ryder, Melanie Subbiah, Jared D Kaplan, Prafulla Dhari-
372 wal, Arvind Neelakantan, Pranav Shyam, Girish Sastry, Amanda Askell, et al. Language
373 models are few-shot learners. *Advances in neural information processing systems*, 33:1877–
374 1901, 2020.

- 375 [16] Tien-Cuong Bui, Van-Duc Le, and Sang-Kyun Cha. A deep learning approach for forecasting
376 air pollution in south korea using lstm. *arXiv preprint arXiv:1804.07891*, 2018.
- 377 [17] Salva Rühling Cachay, Venkatesh Ramesh, Jason NS Cole, Howard Barker, and David Rolnick.
378 Climart: A benchmark dataset for emulating atmospheric radiative transfer in weather and
379 climate models. *arXiv preprint arXiv:2111.14671*, 2021.
- 380 [18] CarbonPlan. CMIP6-Downscaling. [https://github.com/carbonplan/
381 cmip6-downscaling](https://github.com/carbonplan/cmip6-downscaling), 2022.
- 382 [19] Kang Chen, Tao Han, Junchao Gong, Lei Bai, Fenghua Ling, Jing-Jia Luo, Xi Chen, Leiming
383 Ma, Tianning Zhang, Rui Su, et al. Fengwu: Pushing the skillful global medium-range weather
384 forecast beyond 10 days lead. *arXiv preprint arXiv:2304.02948*, 2023.
- 385 [20] Lei Chen, Xiaohui Zhong, Feng Zhang, Yuan Cheng, Yinghui Xu, Yuan Qi, and Hao Li.
386 Fuxi: a cascade machine learning forecasting system for 15-day global weather forecast. *npj
387 Climate and Atmospheric Science*, 6(1):190, 2023. doi: 10.1038/s41612-023-00512-1. URL
388 <https://doi.org/10.1038/s41612-023-00512-1>.
- 389 [21] Lei Chen, Xiaohui Zhong, Feng Zhang, Yuan Cheng, Yinghui Xu, Yuan Qi, and Hao Li. FuXi:
390 A cascade machine learning forecasting system for 15-day global weather forecast. *arXiv
391 preprint arXiv:2306.12873*, 2023.
- 392 [22] Christian Schroeder de Witt, Catherine Tong, Valentina Zantedeschi, Daniele De Martini,
393 Freddie Kalaitzis, Matthew Chantry, Duncan Watson-Parris, and Piotr Bilinski. Rainbench:
394 Towards global precipitation forecasting from satellite imagery, 2020.
- 395 [23] V. Eyring, S. Bony, G. A. Meehl, C. A. Senior, B. Stevens, R. J. Stouffer, and K. E. Taylor.
396 Overview of the Coupled Model Intercomparison Project Phase 6 (CMIP6) experimental design
397 and organization. *Geoscientific Model Development*, 9(5):1937–1958, 2016. doi: 10.5194/
398 gmd-9-1937-2016. URL <https://gmd.copernicus.org/articles/9/1937/2016/>.
- 399 [24] Veronika Eyring, Sandrine Bony, Gerald A Meehl, Catherine A Senior, Bjorn Stevens, Ronald J
400 Stouffer, and Karl E Taylor. Overview of the coupled model intercomparison project phase
401 6 (cmip6) experimental design and organization. *Geoscientific Model Development*, 9(5):
402 1937–1958, 2016.
- 403 [25] Gabriele Franch, Valerio Maggio, Luca Coviello, Marta Pendesini, Giuseppe Jurman, and Ce-
404 sare Furlanello. Taasrad19, a high-resolution weather radar reflectivity dataset for precipitation
405 nowcasting. *Scientific Data*, 7, 07 2020. doi: 10.1038/s41597-020-0574-8.
- 406 [26] Leo Gao, Jonathan Tow, Baber Abbasi, Stella Biderman, Sid Black, Anthony DiPofi, Charles
407 Foster, Laurence Golding, Jeffrey Hsu, Alain Le Noac’h, Haonan Li, Kyle McDonell, Niklas
408 Muennighoff, Chris Ociepa, Jason Phang, Laria Reynolds, Hailey Schoelkopf, Aviya Skowron,
409 Lintang Sutawika, Eric Tang, Anish Thite, Ben Wang, Kevin Wang, and Andy Zou. A
410 framework for few-shot language model evaluation, 12 2023. URL [https://zenodo.org/
411 records/10256836](https://zenodo.org/records/10256836).
- 412 [27] Andrew Geiss, Sam J Silva, and Joseph C Hardin. Downscaling atmospheric chemistry
413 simulations with physically consistent deep learning. *Geoscientific Model Development*, 15
414 (17):6677–6694, 2022.
- 415 [28] Isaac Godfried, Kriti Mahajan, Maggie Wang, Kevin Li, and Pranjalya Tiwari. Flowdb a large
416 scale precipitation, river, and flash flood dataset, 2020.
- 417 [29] Jayesh K Gupta and Johannes Brandstetter. Towards multi-spatiotemporal-scale generalized
418 pde modeling. *arXiv preprint arXiv:2209.15616*, 2022.
- 419 [30] Joseph Hamman and Julia Kent. Scikit-downscale: an open source python package for scalable
420 climate downscaling. In *2020 EarthCube Annual Meeting*, 2020.
- 421 [31] Abderrachid Hamrani, Abdolhamid Akbarzadeh, and Chandra A Madramootoo. Machine
422 learning for predicting greenhouse gas emissions from agricultural soils. *Science of The Total
423 Environment*, 741:140338, 2020.

- 424 [32] Charles R. Harris, K. Jarrod Millman, Stéfan J. van der Walt, Ralf Gommers, Pauli Virtanen,
425 David Cournapeau, Eric Wieser, Julian Taylor, Sebastian Berg, Nathaniel J. Smith, Robert
426 Kern, Matti Picus, Stephan Hoyer, Marten H. van Kerkwijk, Matthew Brett, Allan Haldane,
427 Jaime Fernández del Río, Mark Wiebe, Pearu Peterson, Pierre Gérard-Marchant, Kevin
428 Sheppard, Tyler Reddy, Warren Weckesser, Hameer Abbasi, Christoph Gohlke, and Travis E.
429 Oliphant. Array programming with NumPy. *Nature*, 585(7825):357–362, September 2020. doi:
430 10.1038/s41586-020-2649-2. URL <https://doi.org/10.1038/s41586-020-2649-2>.
- 431 [33] Maximilian Herde, Bogdan Raonić, Tobias Rohner, Roger Käppeli, Roberto Molinaro, Em-
432 manuel de Bézenac, and Siddhartha Mishra. Poseidon: Efficient foundation models for pdes.
433 *arXiv preprint arXiv:2405.19101*, 2024.
- 434 [34] Hans Hersbach, Bill Bell, Paul Berrisford, Shoji Hirahara, András Horányi, Joaquín Muñoz-
435 Sabater, Julien Nicolas, Carole Peubey, Raluca Radu, Dinand Schepers, Adrian Simmons,
436 Cornel Soci, Saleh Abdalla, Xavier Abellan, Gianpaolo Balsamo, Peter Bechtold, Gionata
437 Biavati, Jean Bidlot, Massimo Bonavita, Giovanna De Chiara, Per Dahlgren, Dick Dee, Michail
438 Diamantakis, Rossana Dragani, Johannes Flemming, Richard Forbes, Manuel Fuentes, Alan
439 Geer, Leo Haimberger, Sean Healy, Robin J. Hogan, Elías Hólm, Marta Janisková, Sarah
440 Keeley, Patrick Laloyaux, Philippe Lopez, Cristina Lupu, Gabor Radnoti, Patricia de Rosnay,
441 Iryna Rozum, Freja Vamborg, Sebastien Villaume, and Jean-Noël Thépaut. The ERA5 global
442 reanalysis. *Quarterly Journal of the Royal Meteorological Society*, 146(730):1999–2049, 2020.
443 ISSN 0035-9009. doi: <https://doi.org/10.1002/qj.3803>.
- 444 [35] Azim Heydari, Meysam Majidi Nezhad, Davide Astiaso Garcia, Farshid Keynia, and Livio
445 De Santoli. Air pollution forecasting application based on deep learning model and optimiza-
446 tion algorithm. *Clean Technologies and Environmental Policy*, pages 1–15, 2022.
- 447 [36] Stephan Hoyer and Joe Hamman. xarray: N-D labeled arrays and datasets in Python. *Journal*
448 *of Open Research Software*, 5(1):10, April 2017. doi: 10.5334/jors.148.
- 449 [37] Julia Kaltenborn, Charlotte Lange, Venkatesh Ramesh, Philippe Brouillard, Yaniv Gurwicz,
450 Chandni Nagda, Jakob Runge, Peer Nowack, and David Rolnick. Climateset: A large-scale
451 climate model dataset for machine learning. *Advances in Neural Information Processing*
452 *Systems*, 36:21757–21792, 2023.
- 453 [38] Ryan Keisler. Forecasting global weather with graph neural networks. *arXiv preprint*
454 *arXiv:2202.07575*, 2022.
- 455 [39] Christoph A Keller, K Emma Knowland, Bryan N Duncan, Junhua Liu, Daniel C Anderson,
456 Sampa Das, Robert A Lucchesi, Elizabeth W Lundgren, Julie M Nicely, Eric Nielsen, et al.
457 Description of the nasa geos composition forecast modeling system geos-cf v1. 0. *Journal of*
458 *Advances in Modeling Earth Systems*, 13(4):e2020MS002413, 2021.
- 459 [40] K Emma Knowland, Christoph A Keller, Pamela A Wales, Krzysztof Wargan, Lawrence Coy,
460 Matthew S Johnson, Junhua Liu, Robert A Lucchesi, Sebastian David Eastham, E Fleming, et al.
461 Nasa geos composition forecast modeling system geos-cf v1. 0: Stratospheric composition.
462 *Journal of advances in modeling earth systems*, 14(6):e2021MS002852, 2022.
- 463 [41] Dmitrii Kochkov, Janni Yuval, Ian Langmore, Peter Norgaard, Jamie Smith, Griffin Mooers,
464 James Lottes, Stephan Rasp, Peter Düben, Milan Klöwer, et al. Neural general circulation
465 models. *arXiv preprint arXiv:2311.07222*, 2023.
- 466 [42] Dmitrii Kochkov, Janni Yuval, Ian Langmore, Peter Norgaard, Jamie Smith, Griffin Mooers,
467 Milan Klöwer, James Lottes, Stephan Rasp, Peter Düben, Sam Hatfield, Peter Battaglia, Alvaro
468 Sanchez-Gonzalez, Matthew Willson, Michael P. Brenner, and Stephan Hoyer. Neural general
469 circulation models for weather and climate, 2024.
- 470 [43] Romain Lacombe, Hannah Grossman, Lucas Hendren, and David Lüdeke. Improving extreme
471 weather events detection with light-weight neural networks. *arXiv preprint arXiv:2304.00176*,
472 2023.

- 473 [44] Remi Lam, Alvaro Sanchez-Gonzalez, Matthew Willson, Peter Wirmsberger, Meire Fortunato,
474 Ferran Alet, Suman Ravuri, Timo Ewalds, Zach Eaton-Rosen, Weihua Hu, Alexander Merose,
475 Stephan Hoyer, George Holland, Oriol Vinyals, Jacklynn Stott, Alexander Pritzel, Shakir
476 Mohamed, and Peter Battaglia. Learning skillful medium-range global weather forecasting.
477 *Science*, 0(0):eadi2336, 2023. doi: 10.1126/science.adi2336. URL <https://www.science.org/doi/abs/10.1126/science.adi2336>.
- 479 [45] David A. Lavers, Adrian Simmons, Freja Vamborg, and Mark J. Rodwell. An evaluation of
480 ERA5 precipitation for climate monitoring. *Quarterly Journal of the Royal Meteorological
481 Society*, 148(748):3152–3165, 2022. doi: <https://doi.org/10.1002/qj.4351>. URL <https://rmets.onlinelibrary.wiley.com/doi/abs/10.1002/qj.4351>.
- 483 [46] L. Ruby Leung, Linda O. Mearns, Filippo Giorgi, and Robert L. Wilby. REGIONAL CLIMATE
484 RESEARCH: Needs and Opportunities. *Bulletin of the American Meteorological Society*,
485 84(1):89–95, 2003. ISSN 00030007, 15200477. URL <http://www.jstor.org/stable/26215433>.
- 487 [47] Percy Liang, Rishi Bommasani, Tony Lee, Dimitris Tsipras, Dilara Soylu, Michihiro Yasunaga,
488 Yian Zhang, Deepak Narayanan, Yuhuai Wu, Ananya Kumar, et al. Holistic evaluation of
489 language models. *arXiv preprint arXiv:2211.09110*, 2022.
- 490 [48] Yumin Liu, Auroop R. Ganguly, and Jennifer Dy. Climate Downscaling Using YNet: A
491 Deep Convolutional Network with Skip Connections and Fusion. In *Proceedings of the 26th
492 ACM SIGKDD International Conference on Knowledge Discovery and Data Mining, KDD
493 '20*, page 3145–3153, New York, NY, USA, 2020. Association for Computing Machinery.
494 ISBN 9781450379984. doi: 10.1145/3394486.3403366. URL <https://doi.org/10.1145/3394486.3403366>.
- 496 [49] Pan Lu, Hritik Bansal, Tony Xia, Jiacheng Liu, Chunyuan Li, Hannaneh Hajishirzi, Hao
497 Cheng, Kai-Wei Chang, Michel Galley, and Jianfeng Gao. Mathvista: Evaluating mathematical
498 reasoning of foundation models in visual contexts. *arXiv preprint arXiv:2310.02255*, 2023.
- 499 [50] Peter Lynch. The origins of computer weather prediction and climate modeling. *Journal of
500 computational physics*, 227(7):3431–3444, 2008.
- 501 [51] Manil Maskey, Rahul Ramachandran, Muthukumaran Ramasubramanian, Iksha Gurung, Brian
502 Freitag, Aaron Kaulfus, Drew Bollinger, Daniel Cecil, and J. Miller. Deepti: Deep-learning-
503 based tropical cyclone intensity estimation system. *IEEE Journal of Selected Topics in Applied
504 Earth Observations and Remote Sensing*, PP:1–1, 07 2020. doi: 10.1109/JSTARS.2020.
505 3011907.
- 506 [52] Michael McCabe, Bruno Régaldo-Saint Blancard, Liam Holden Parker, Ruben Ohana, Miles
507 Cranmer, Alberto Bietti, Michael Eickenberg, Siavash Golkar, Geraud Krawezik, Francois
508 Lanusse, et al. Multiple physics pretraining for physical surrogate models. *arXiv preprint
509 arXiv:2310.02994*, 2023.
- 510 [53] Christoph Minixhofer, Mark Swan, Calum McMeekin, and Pavlos Andreadis. Droughted: A
511 dataset and methodology for drought forecasting spanning multiple climate zones. In *ICML
512 2021 Workshop on Tackling Climate Change with Machine Learning*, 2021.
- 513 [54] Soukayna Mouatadid, Paulo Orenstein, Genevieve Flaspohler, Judah Cohen, Miruna Oprescu,
514 Ernest Fraenkel, and Lester Mackey. Adaptive bias correction for improved subseasonal
515 forecasting. *Nature Communications*, 14(1), June 2023. ISSN 2041-1723. doi: 10.1038/
516 s41467-023-38874-y. URL <http://dx.doi.org/10.1038/s41467-023-38874-y>.
- 517 [55] Soukayna Mouatadid, Paulo Orenstein, Genevieve Flaspohler, Miruna Oprescu, Judah Cohen,
518 Franklyn Wang, Sean Knight, Maria Geogdzhayeva, Sam Levang, Ernest Fraenkel, and Lester
519 Mackey. Subseasonalclimateusa: A dataset for subseasonal forecasting and benchmarking,
520 2024.
- 521 [56] Takeyoshi Nagasato, Kei Ishida, Ali Ercan, Tongbi Tu, Masato Kiyama, Motoki Amagasaki,
522 and Kazuki Yokoo. Extension of convolutional neural network along temporal and vertical
523 directions for precipitation downscaling. *arXiv preprint arXiv:2112.06571*, 2021.

- 524 [57] Juan Nathaniel, Yongquan Qu, Tung Nguyen, Sungduk Yu, Julius Busecke, Aditya Grover,
525 and Pierre Gentine. Chaosbench: A multi-channel, physics-based benchmark for subseasonal-
526 to-seasonal climate prediction. *arXiv preprint arXiv:2402.00712*, 2024.
- 527 [58] Grey Nearing, Deborah Cohen, Vusumuzi Dube, Martin Gauch, Oren Gilon, Shaun Harrigan,
528 Avinatan Hassidim, Daniel Klotz, Frederik Kratzert, Asher Metzger, and et al. Global predic-
529 tion of extreme floods in ungauged watersheds. *Nature*, 627(8004):559–563, Mar 2024. doi:
530 10.1038/s41586-024-07145-1.
- 531 [59] Tung Nguyen, Johannes Brandstetter, Ashish Kapoor, Jayesh K Gupta, and Aditya Grover.
532 ClimaX: A foundation model for weather and climate. *arXiv preprint arXiv:2301.10343*, 2023.
- 533 [60] Tung Nguyen, Jason Jewik, Hritik Bansal, Prakhar Sharma, and Aditya Grover. Climate-
534 learn: Benchmarking machine learning for weather and climate modeling. *arXiv preprint*
535 *arXiv:2307.01909*, 2023.
- 536 [61] Tung Nguyen, Rohan Shah, Hritik Bansal, Troy Arcomano, Sandeep Madireddy, Romit Maulik,
537 Veerabhadra Kotamarthi, Ian Foster, and Aditya Grover. Scaling transformer neural networks
538 for skillful and reliable medium-range weather forecasting. *arXiv preprint arXiv:2312.03876*,
539 2023.
- 540 [62] Adam Paszke, Sam Gross, Francisco Massa, Adam Lerer, James Bradbury, Gregory Chanan,
541 Trevor Killeen, Zeming Lin, Natalia Gimelshein, Luca Antiga, Alban Desmaison, Andreas
542 Kopf, Edward Yang, Zachary DeVito, Martin Raison, Alykhan Tejani, Sasank Chilamkurthy,
543 Benoit Steiner, Lu Fang, Junjie Bai, and Soumith Chintala. Pytorch: An imperative style, high-
544 performance deep learning library. In *Advances in Neural Information Processing Systems*
545 (*NeurIPS*), pages 8024–8035. Curran Associates, Inc., 2019.
- 546 [63] Jaideep Pathak, Shashank Subramanian, Peter Harrington, Sanjeev Raja, Ashesh Chattopad-
547 hyay, Morteza Mardani, Thorsten Kurth, David Hall, Zongyi Li, Kamyar Azizzadenesheli,
548 et al. Fourcastnet: A global data-driven high-resolution weather model using adaptive fourier
549 neural operators. *arXiv preprint arXiv:2202.11214*, 2022.
- 550 [64] Jaideep Pathak, Shashank Subramanian, Peter Harrington, Sanjeev Raja, Ashesh Chattopad-
551 hyay, Morteza Mardani, Thorsten Kurth, David Hall, Zongyi Li, Kamyar Azizzadenesheli,
552 et al. Fourcastnet: A global data-driven high-resolution weather model using adaptive fourier
553 neural operators. *arXiv preprint arXiv:2202.11214*, 2022.
- 554 [65] Andrew D Polasky, Jenni L Evans, and Jose D Fuentes. Ccdownscaling: A python package for
555 multivariable statistical climate model downscaling. *Environmental Modelling & Software*,
556 165:105712, 2023.
- 557 [66] Prabhat, Karthik Kashinath, Mayur Mudigonda, Sol Kim, Lukas Kapp-Schwoerer, Andre
558 Graubner, Ege Karaismailoglu, Leo von Kleist, Thorsten Kurth, Annette Greiner, et al. Cli-
559 matenet: An expert-labelled open dataset and deep learning architecture for enabling high-
560 precision analyses of extreme weather. *Geoscientific Model Development Discussions*, 2020:
561 1–28, 2020.
- 562 [67] Prabhat, K. Kashinath, M. Mudigonda, S. Kim, L. Kapp-Schwoerer, A. Graubner, E. Karais-
563 mailoglu, L. von Kleist, T. Kurth, A. Greiner, A. Mahesh, K. Yang, C. Lewis, J. Chen,
564 A. Lou, S. Chandran, B. Toms, W. Chapman, K. Dagon, C. A. Shields, T. O’Brien,
565 M. Wehner, and W. Collins. Climatednet: an expert-labeled open dataset and deep learn-
566 ing architecture for enabling high-precision analyses of extreme weather. *Geoscientific*
567 *Model Development*, 14(1):107–124, 2021. doi: 10.5194/gmd-14-107-2021. URL <https://gmd.copernicus.org/articles/14/107/2021/>.
- 569 [68] Ilan Price, Alvaro Sanchez-Gonzalez, Ferran Alet, Tom R. Andersson, Andrew El-Kadi,
570 Dominic Masters, Timo Ewalds, Jacklynn Stott, Shakir Mohamed, Peter Battaglia, Remi Lam,
571 and Matthew Willson. Gencast: Diffusion-based ensemble forecasting for medium-range
572 weather, 2024.
- 573 [69] Adiba Mahbub Proma, Md Saiful Islam, Stela Ciko, Raiyan Abdul Baten, and Ehsan Hoque.
574 Nadbenchmarks—a compilation of benchmark datasets for machine learning tasks related to
575 natural disasters. *arXiv preprint arXiv:2212.10735*, 2022.

- 576 [70] Evan Racah, Christopher Beckham, Tegan Maharaj, Samira Ebrahimi Kahou, Mr. Prab-
577 hat, and Chris Pal. Extremeweather: A large-scale climate dataset for semi-supervised de-
578 tection, localization, and understanding of extreme weather events. In I. Guyon, U. Von
579 Luxburg, S. Bengio, H. Wallach, R. Fergus, S. Vishwanathan, and R. Garnett, editors,
580 *Advances in Neural Information Processing Systems*, volume 30. Curran Associates, Inc.,
581 2017. URL [https://proceedings.neurips.cc/paper_files/paper/2017/file/
582 519c84155964659375821f7ca576f095-Paper.pdf](https://proceedings.neurips.cc/paper_files/paper/2017/file/519c84155964659375821f7ca576f095-Paper.pdf).
- 583 [71] Alec Radford, Jong Wook Kim, Chris Hallacy, Aditya Ramesh, Gabriel Goh, Sandhini Agarwal,
584 Girish Sastry, Amanda Askell, Pamela Mishkin, Jack Clark, et al. Learning transferable visual
585 models from natural language supervision. In *International Conference on Machine Learning*,
586 pages 8748–8763. PMLR, 2021.
- 587 [72] Maryam Rahnemoonfar, Tashnim Chowdhury, Argho Sarkar, Debvrat Varshney, Masoud Yari,
588 and Robin Roberson Murphy. Floodnet: A high resolution aerial imagery dataset for post flood
589 scene understanding. *IEEE Access*, 9:89644–89654, 2021.
- 590 [73] Stephan Rasp and Nils Thuerey. Data-driven medium-range weather prediction with a resnet
591 pretrained on climate simulations: A new model for weatherbench. *Journal of Advances in
592 Modeling Earth Systems*, 13(2):e2020MS002405, 2021.
- 593 [74] Stephan Rasp, Peter D Dueben, Sebastian Scher, Jonathan A Weyn, Soukayna Mouatadid,
594 and Nils Thuerey. Weatherbench: a benchmark data set for data-driven weather forecasting.
595 *Journal of Advances in Modeling Earth Systems*, 12(11):e2020MS002203, 2020.
- 596 [75] Stephan Rasp, Hauke Schulz, Sandrine Bony, and Bjorn Stevens. Combining crowd-sourcing
597 and deep learning to explore the meso-scale organization of shallow convection, 2020.
- 598 [76] Stephan Rasp, Stephan Hoyer, Alexander Merose, Ian Langmore, Peter Battaglia, Tyler Russel,
599 Alvaro Sanchez-Gonzalez, Vivian Yang, Rob Carver, Shreya Agrawal, Matthew Chantry,
600 Zied Ben Bouallegue, Peter Dueben, Carla Bromberg, Jared Sisk, Luke Barrington, Aaron
601 Bell, and Fei Sha. Weatherbench 2: A benchmark for the next generation of data-driven global
602 weather models, 2023.
- 603 [77] Sara A. Rauscher, Erika Coppola, Claudio Piani, and Filippo Giorgi. Resolution effects on
604 regional climate model simulations of seasonal precipitation over Europe. *Climate Dynamics*,
605 35(4):685–711, Sep 2010. ISSN 1432-0894. doi: 10.1007/s00382-009-0607-7. URL <https://doi.org/10.1007/s00382-009-0607-7>.
- 607 [78] Suman Ravuri, Karel Lenc, Matthew Willson, Dmitry Kangin, Remi Lam, Piotr Mirowski,
608 Megan Fitzsimons, Maria Athanassiadou, Sheleem Kashem, Sam Madge, Rachel Prudden,
609 Amol Mandhane, Aidan Clark, Andrew Brock, Karen Simonyan, Raia Hadsell, Niall Robinson,
610 Ellen Clancy, Alberto Arribas, and Shakir Mohamed. Skilful precipitation nowcasting using
611 deep generative models of radar. *Nature*, 597(7878):672–677, Sep 2021. ISSN 1476-4687. doi:
612 10.1038/s41586-021-03854-z. URL <https://doi.org/10.1038/s41586-021-03854-z>.
- 613 [79] Suman Ravuri, Karel Lenc, Matthew Willson, Dmitry Kangin, Remi Lam, Piotr Mirowski,
614 Megan Fitzsimons, Maria Athanassiadou, Sheleem Kashem, Sam Madge, et al. Skilful
615 precipitation nowcasting using deep generative models of radar. *Nature*, 597(7878):672–677,
616 2021.
- 617 [80] Christian Requena-Mesa, Vitus Benson, Markus Reichstein, Jakob Runge, and Joachim
618 Denzler. Earthnet2021: A large-scale dataset and challenge for earth surface forecasting as
619 a guided video prediction task. In *Proceedings of the IEEE/CVF Conference on Computer
620 Vision and Pattern Recognition*, pages 1132–1142, 2021.
- 621 [81] Eduardo Rocha Rodrigues, Igor Oliveira, Renato Cunha, and Marco Netto. Deepdownscale: A
622 deep learning strategy for high-resolution weather forecast. In *2018 IEEE 14th International
623 Conference on e-Science (e-Science)*, pages 415–422. IEEE, 2018.
- 624 [82] Robert A Rohde and Zeke Hausfather. The berkeley earth land/ocean temperature record.
625 *Earth System Science Data*, 12(4):3469–3479, 2020.

- 626 [83] Olaf Ronneberger, Philipp Fischer, and Thomas Brox. U-net: Convolutional networks
627 for biomedical image segmentation. In *Medical Image Computing and Computer-Assisted*
628 *Intervention–MICCAI 2015: 18th International Conference, Munich, Germany, October 5-9,*
629 *2015, Proceedings, Part III 18*, pages 234–241. Springer, 2015.
- 630 [84] DA Sachindra, Khandakar Ahmed, Md Mamunur Rashid, S Shahid, and BJC Perera. Statistical
631 downscaling of precipitation using machine learning techniques. *Atmospheric research*, 212:
632 240–258, 2018.
- 633 [85] Øyvind Seland, Mats Bentsen, Dirk Jan Leo Olivière, Thomas Toniazzo, Ada Gjermundsen,
634 Lise Seland Graff, Jens Boldingh Debernard, Alok Kumar Gupta, Yan-Chun He, Alf Kirkevåg,
635 et al. Overview of the norwegian earth system model (noresm2) and key climate response of
636 cmp6 deck, historical, and scenario simulations. 2020.
- 637 [86] Muhammed Sit, Bong-Chul Seo, and Ibrahim Demir. Iowarain: A statewide rain event
638 dataset based on weather radars and quantitative precipitation estimation. *arXiv preprint*
639 *arXiv:2107.03432*, 2021.
- 640 [87] Casper Kaae Sønderby, Lasse Espeholt, Jonathan Heek, Mostafa Dehghani, Avital Oliver, Tim
641 Salimans, Shreya Agrawal, Jason Hickey, and Nal Kalchbrenner. MetNet: A neural weather
642 model for precipitation forecasting. *arXiv preprint arXiv:2003.12140*, 2020.
- 643 [88] Aarohi Srivastava, Abhinav Rastogi, Abhishek Rao, Abu Awal Md Shoeb, Abubakar Abid,
644 Adam Fisch, Adam R Brown, Adam Santoro, Aditya Gupta, Adrià Garriga-Alonso, et al.
645 Beyond the imitation game: Quantifying and extrapolating the capabilities of language models.
646 *arXiv preprint arXiv:2206.04615*, 2022.
- 647 [89] Jingmin Sun, Yuxuan Liu, Zecheng Zhang, and Hayden Schaeffer. Towards a foundation model
648 for partial differential equation: Multi-operator learning and extrapolation. *arXiv preprint*
649 *arXiv:2404.12355*, 2024.
- 650 [90] Qing Tao, Fang Liu, Yong Li, and Denis Sidorov. Air pollution forecasting using a deep
651 learning model based on 1d convnets and bidirectional gru. *IEEE access*, 7:76690–76698,
652 2019.
- 653 [91] Thomas Vandal, Evan Kodra, and Auroop R Ganguly. Intercomparison of machine learning
654 methods for statistical downscaling: the case of daily and extreme precipitation. *Theoretical*
655 *and Applied Climatology*, 137:557–570, 2019.
- 656 [92] Ashish Vaswani, Noam Shazeer, Niki Parmar, Jakob Uszkoreit, Llion Jones, Aidan N Gomez,
657 Łukasz Kaiser, and Illia Polosukhin. Attention is all you need. *Advances in Neural Information*
658 *Processing Systems*, 30, 2017.
- 659 [93] Francisco Villaescusa-Navarro, Shy Genel, Daniel Anglés-Alcázar, Leander Thiele, Romeel
660 Dave, Desika Narayanan, Andrina Nicola, Yin Li, Pablo Villanueva-Domingo, Benjamin
661 Wandelt, David N. Spergel, Rachel S. Somerville, Jose Manuel Zorrilla Matilla, Faizan G.
662 Mohammad, Sultan Hassan, Helen Shao, Digvijay Wadekar, Michael Eickenberg, Kaze W. K.
663 Wong, Gabriella Contardo, Yongseok Jo, Emily Moser, Erwin T. Lau, Luis Fernando Machado
664 Poletti Valle, Lucia A. Perez, Daisuke Nagai, Nicholas Battaglia, and Mark Vogelsberger.
665 The camels multifield data set: Learning the universe’s fundamental parameters with artificial
666 intelligence. *The Astrophysical Journal Supplement Series*, 259(2):61, April 2022. ISSN 1538-
667 4365. doi: 10.3847/1538-4365/ac5ab0. URL [http://dx.doi.org/10.3847/1538-4365/
668 ac5ab0](http://dx.doi.org/10.3847/1538-4365/ac5ab0).
- 669 [94] F. Vitart, A. W. Robertson, A. Spring, F. Pinault, R. Roškar, W. Cao, S. Bech, A. Bienkowski,
670 N. Caltabiano, E. De Coning, B. Denis, A. Dirkson, J. Dramsch, P. Dueben, J. Gierschendorf,
671 H. S. Kim, K. Nowak, D. Landry, L. Lledó, L. Palma, S. Rasp, and S. Zhou. Outcomes of the
672 WMO prize challenge to improve subseasonal to seasonal predictions using artificial intelli-
673 gence. *Bulletin of the American Meteorological Society*, 103(12):E2878–E2886, December
674 2022. doi: 10.1175/bams-d-22-0046.1.
- 675 [95] Frédéric Vitart and Andrew W Robertson. The sub-seasonal to seasonal prediction project
676 (s2s) and the prediction of extreme events. *npj Climate and Atmospheric Science*, 1(1):1–7,
677 2018.

- 678 [96] Xiaoxuan Wang, Ziniu Hu, Pan Lu, Yanqiao Zhu, Jieyu Zhang, Satyen Subramaniam, Arjun R
679 Loomba, Shichang Zhang, Yizhou Sun, and Wei Wang. Scibench: Evaluating college-level
680 scientific problem-solving abilities of large language models. *arXiv preprint arXiv:2307.10635*,
681 2023.
- 682 [97] D. Watson-Parris, Y. Rao, D. Olivié, Ø. Seland, P. Nowack, G. Camps-Valls, P. Stier,
683 S. Bouabid, M. Dewey, E. Fons, J. Gonzalez, P. Harder, K. Jeggle, J. Lenhardt,
684 P. Manshausen, M. Novitasari, L. Ricard, and C. Roesch. ClimateBench v1.0:
685 A Benchmark for Data-Driven Climate Projections. *Journal of Advances in Mod-
686 eling Earth Systems*, 14(10):e2021MS002954, 2022. doi: [https://doi.org/10.1029/
687 2021MS002954](https://doi.org/10.1029/2021MS002954). URL [https://agupubs.onlinelibrary.wiley.com/doi/abs/10.
688 1029/2021MS002954](https://agupubs.onlinelibrary.wiley.com/doi/abs/10.1029/2021MS002954). e2021MS002954 2021MS002954.
- 689 [98] Duncan Watson-Parris, Yuhang Rao, Dirk Olivié, Øyvind Seland, Peer Nowack, Gustau Camps-
690 Valls, Philip Stier, Shahine Bouabid, Maura Dewey, Emilie Fons, et al. Climatebench v1. 0:
691 A benchmark for data-driven climate projections. *Journal of Advances in Modeling Earth
692 Systems*, 14(10):e2021MS002954, 2022.
- 693 [99] Oliver Watt-Meyer, Gideon Dresdner, Jeremy McGibbon, Spencer K. Clark, Brian Henn,
694 James Duncan, Noah D. Brenowitz, Karthik Kashinath, Michael S. Pritchard, Boris Bonev,
695 Matthew E. Peters, and Christopher S. Bretherton. Ace: A fast, skillful learned global
696 atmospheric model for climate prediction, 2023.
- 697 [100] NP Wedi, P Bauer, W Denoninck, M Diamantakis, M Hamrud, C Kuhnlein, S Malardel,
698 K Mogensen, G Mozdzyński, and PK Smolarkiewicz. *The modelling infrastructure of the
699 Integrated Forecasting System: Recent advances and future challenges*. European Centre for
700 Medium-Range Weather Forecasts, 2015.
- 701 [101] Jonathan A Weyn, Dale R Durran, and Rich Caruana. Improving data-driven global weather
702 prediction using deep convolutional neural networks on a cubed sphere. *Journal of Advances
703 in Modeling Earth Systems*, 12(9):e2020MS002109, 2020.
- 704 [102] Ross Wightman. PyTorch image models. [https://github.com/rwightman/
705 pytorch-image-models](https://github.com/rwightman/pytorch-image-models), 2019.
- 706 [103] T Wu, S Tang, R Zhang, J Cao, and Y Zhang Cgnet. A light-weight context guided network
707 for semantic segmentation., 2020, 30. DOI: <https://doi.org/10.1109/TIP>, pages 1169–1179,
708 2020.
- 709 [104] Sungduk Yu, Walter Hannah, Liran Peng, Jerry Lin, Mohamed Aziz Bhouiri, Ritwik Gupta,
710 Björn Lütjens, Justus Christopher Will, Gunnar Behrens, Julius Busecke, Nora Loose, Charles I
711 Stern, Tom Beucler, Bryce Harrop, Benjamin R Hillman, Andrea Jenney, Savannah Ferretti,
712 Nana Liu, Anima Anandkumar, Noah D Brenowitz, Veronika Eyring, Nicholas Geneva, Pierre
713 Gentine, Stephan Mandt, Jaideep Pathak, Akshay Subramaniam, Carl Vondrick, Rose Yu, Laure
714 Zanna, Tian Zheng, Ryan Abernathy, Fiaz Ahmed, David C Bader, Pierre Baldi, Elizabeth
715 Barnes, Christopher Bretherton, Peter Caldwell, Wayne Chuang, Yilun Han, Yu Huang,
716 Fernando Iglesias-Suarez, Sanket Jantre, Karthik Kashinath, Marat Khairoutdinov, Thorsten
717 Kurth, Nicholas Lutsko, Po-Lun Ma, Griffin Mooers, J. David Neelin, David Randall, Sara
718 Shamekh, Mark A Taylor, Nathan Urban, Janni Yuval, Guang Zhang, and Michael Pritchard.
719 Climsim: A large multi-scale dataset for hybrid physics-ml climate emulation, 2024.
- 720 [105] Xiang Yue, Yuansheng Ni, Kai Zhang, Tianyu Zheng, Ruoqi Liu, Ge Zhang, Samuel
721 Stevens, Dongfu Jiang, Weiming Ren, Yuxuan Sun, et al. Mmmu: A massive multi-
722 discipline multimodal understanding and reasoning benchmark for expert agi. *arXiv preprint
723 arXiv:2311.16502*, 2023.
- 724 [106] Yuchen Zhang, Mingsheng Long, Kaiyuan Chen, Lanxiang Xing, Ronghua Jin, Michael I.
725 Jordan, and Jianmin Wang. Skillful nowcasting of extreme precipitation with nowcastnet.
726 *Nature*, 619(7970):526–532, Jul 2023. doi: 10.1038/s41586-023-06184-4.

727 **Checklist**

- 728 1. For all authors...
- 729 (a) Do the main claims made in the abstract and introduction accurately reflect the paper’s
730 contributions and scope? [Yes] The abstract and introduction reflect our contribution of
731 proposing AtmosArena, a benchmark for evaluating foundation models in atmospheric
732 sciences.
- 733 (b) Did you describe the limitations of your work? [Yes] See Section 5.
- 734 (c) Did you discuss any potential negative societal impacts of your work? [NA] Our work
735 does not have potential negative societal impacts.
- 736 (d) Have you read the ethics review guidelines and ensured that your paper conforms to
737 them? [Yes] The paper conforms to the ethics review guidelines.
- 738 2. If you are including theoretical results...
- 739 (a) Did you state the full set of assumptions of all theoretical results? [NA] The paper does
740 not include theoretical results.
- 741 (b) Did you include complete proofs of all theoretical results? [NA] The paper does not
742 include theoretical results.
- 743 3. If you ran experiments (e.g. for benchmarks)...
- 744 (a) Did you include the code, data, and instructions needed to reproduce the main experi-
745 mental results (either in the supplemental material or as a URL)? [Yes] The benchmark
746 is publically available at <https://github.com/tung-nd/atmos-arena>.
- 747 (b) Did you specify all the training details (e.g., data splits, hyperparameters, how they
748 were chosen)? [Yes] See Section 3 and Appendix D.
- 749 (c) Did you report error bars (e.g., with respect to the random seed after running experi-
750 ments multiple times)? [No] It is too computationally expensive and not a common
751 practice in this domain.
- 752 (d) Did you include the total amount of compute and the type of resources used (e.g., type
753 of GPUs, internal cluster, or cloud provider)? [Yes] See Section D.
- 754 4. If you are using existing assets (e.g., code, data, models) or curating/releasing new assets...
- 755 (a) If your work uses existing assets, did you cite the creators? [Yes] We cited the creators.
- 756 (b) Did you mention the license of the assets? [Yes] We mentioned the license of the
757 datasets.
- 758 (c) Did you include any new assets either in the supplemental material or as a URL? [No]
759 We do not.
- 760 (d) Did you discuss whether and how consent was obtained from people whose data you’re
761 using/curating? [NA] Not applicable to our work.
- 762 (e) Did you discuss whether the data you are using/curating contains personally identifiable
763 information or offensive content? [NA] Not applicable to our work.
- 764 5. If you used crowdsourcing or conducted research with human subjects...
- 765 (a) Did you include the full text of instructions given to participants and screenshots, if
766 applicable? [NA] Not applicable to our work.
- 767 (b) Did you describe any potential participant risks, with links to Institutional Review
768 Board (IRB) approvals, if applicable? [NA] Not applicable to our work.
- 769 (c) Did you include the estimated hourly wage paid to participants and the total amount
770 spent on participant compensation? [NA] Not applicable to our work.

771 A Licenses and Terms of Use

772 The source code is available online under the MIT License at [https://github.com/tung-nd/](https://github.com/tung-nd/atmos-arena)
 773 [atmos-arena](https://github.com/tung-nd/atmos-arena). The licenses of the datasets we use in AtmosArena are as follows:

- 774 • ERA5 is curated and provided by WeatherBench2 which is licensed under Apache
 775 License 2.0 ([https://github.com/google-research/weatherbench2/blob/main/](https://github.com/google-research/weatherbench2/blob/main/LICENSE)
 776 [LICENSE](https://github.com/google-research/weatherbench2/blob/main/LICENSE)).
- 777 • Berkeley Earth (<https://berkeleyearth.org/data/>), ClimateBench (<https://zenodo.org/record/7064308>), ClimateNet ([https://gmd.copernicus.org/](https://gmd.copernicus.org/articles/14/107/2021/)
 778 [articles/14/107/2021/](https://gmd.copernicus.org/articles/14/107/2021/)) are available under the CC BY 4.0 license.
- 780 • CAMS Analysis provided by Copernicus Atmosphere Monitoring Service (CAMS) is free
 781 of charge, worldwide, non-exclusive, royalty-free and perpetual ([https://atmosphere.](https://atmosphere.copernicus.eu/sites/default/files/repository/CAMS_data_license.pdf)
 782 [copernicus.eu/sites/default/files/repository/CAMS_data_license.pdf](https://atmosphere.copernicus.eu/sites/default/files/repository/CAMS_data_license.pdf)).
- 783 • GEOS-CF (<https://portal.nccs.nasa.gov/datashare/gmao/geos-cf/>) provided
 784 by NASA is free for public access.

785 B Datasets

786 B.1 Dataset details

Table 5: Summary of the datasets used to finetune and evaluate baselines in AtmosArena.

Name	Resolution	Temporal coverage	Surface Variables	Multi-level Variables	Num levels	Size (GB)	Num frames
ERA5	128x256	1979-2020	T2m, U10, V10, MSLP	Z, T, U, V, Q	13	1600	61,324
Berkeley Earth	128x256	1850-2023	T2m	N/A	N/A	0.26	2,088
ClimateBench	32x64	2015-2100	CO2, SO2, CH4, BC, TAS, DTR, PR, PR90	N/A	N/A	0.12	839
ClimateNet	768x1152	1996-2013	TMQ, UBOT, VBOT, PS, PSL, PRECT, TS, TREFHT, ZBOT	U850, V850, QREFHT, T200, T500, Z1000, Z200	N/A	28	459
CAMS Analysis	128x256	2017-2022	T2m, U10, V10, MSLP, TC CO, TC NO, TC NO2, TC SO2, TC O3, PM1, PM2.5, PM10	U, V, T, Q, Z, CO, NO, NO2, SO2, O3	13	59	3774
GEOS-CF	128x256	2018-2023	NO2, SO2, CO, O3, PM2.5	N/A	N/A	363	52,584

787 Table 5 details the datasets in AtmosArena, including their spatial resolution, temporal coverage,
 788 variables, and size. The full names of the abbreviated variables are:

- 789 • T2m, U10, V10, MSLP: 2-meter temperature, 10-meter zonal wind, 10-meter meridional
 790 wind, Mean sea level pressure.
- 791 • Z, T, U, V, Q: Geopotential, Temperature, Zonal wind, Meridional wind, Specific humidity
 792 at different pressure levels.
- 793 • CO2, SO2, CH4, BC: Carbon dioxide, Sulfur Dioxide, Methane, Black carbon.
- 794 • TAS, DTR, PR, PR90: Surface air temperature, Diurnal temperature range, Precipitation,
 795 90th percentile precipitation.
- 796 • TMQ, UBOT, VBOT, PS, PSL, PRECT, TS, TREFHT, ZBOT: Total Precipitable Water,
 797 Lowest Model Level Zonal Wind, Lowest Model Level Meridional Wind, Surface Pres-
 798 sure, Sea Level Pressure, Total Precipitation Rate, Surface Temperature, Reference Height
 799 Temperature, Lowest Model Level Height.
- 800 • U850, V850, QREFHT, T200, T500, Z1000, Z200: Zonal Wind at 850 mb, Meridional Wind
 801 at 850 mb, Specific Humidity at Reference Height, Temperature at 200 mb, Temperature at
 802 500 mb, Geopotential Height at 1000 mb, Geopotential Height at 200 MB.
- 803 • TC CO, TC NO, TC NO2, TC SO2, TC O3, PM1, PM2.5, PM10: Total Column Carbon
 804 Monoxide, Total Column Nitric Oxide, Total Column Nitrogen Dioxide, Total Column
 805 Sulfur Dioxide, Total Column Ozone, Particulate Matter 1um, Particulate Matter 2.5um,
 806 Particulate Matter 10um.

- CO, NO, NO₂, SO₂, O₃: Zonal Wind, Meridional Wind, Temperature, Specific Humidity, Geopotential Height, Carbon Monoxide, Nitric Oxide, Nitrogen Dioxide, Sulfur Dioxide, Ozone.

For ERA5, following WeatherBench2 [76], we used the 6-hourly subsampled data from the original ERA5 at 00:00, 06:00, 12:00, and 18:00, and used the 13 pressure levels for the multi-level variables: 50, 100, 150, 200, 250, 300, 400, 500, 600, 700, 850, 925, 1000. We use the same pressure levels for CAM Analysis. We also note that the resolutions of ERA5, Berkeley Earth, ClimateBench, CAMS Analysis, and GEOS-RF used in our paper are different from their original resolutions. We used bilinear interpolation to regrid the original data to the resolutions in Table 5.

B.2 Train, validation, and test split

Table 6: Summary of train, validation, and test split of the datasets in AtmosArena.

Name	Train time frame	Validation time frame	Test Year(s)
time frame	1979-2018	2019	2020
Berkeley Earth	N/A	N/A	2000-2024
ClimateBench	2015-2100	2015-2100	2015-2100
ClimateNet	1996-2007	2008-2010	2011-2013
CAMS Analysis	2018-2020	2021	2022
GEOS-CF	2017-2020	2021	2022

Table 6 summarizes the train, validation, and test split of the datasets we included in AtmosArena. Most datasets are split according to time, where training, validation, and test data belong to non-overlapping time periods. For ClimateBench, which we used for the climate model emulation task, however, the data is split according to different future emission scenarios. We refer to ClimateBench [98] for a detailed discussion of these scenarios.

C Evaluation metrics

This section presents the formulation of the evaluation metrics we included in AtmosArena. We use the following notations across the metrics:

- N is the number of data points
- H is the number of latitude coordinates.
- W is the number of longitude coordinates.
- X and \tilde{X} are the ground-truth and prediction, respectively.

Each equation below is computed for one single variable. To account for the non-uniformity of the grid cell areas when gridding a round Earth, most metrics are latitude-weighted to give more weight to the cells closer to the equator. The latitude weighting function is given by

$$L(i) = \frac{\cos(H_i)}{\frac{1}{H} \sum_{i=1}^H \cos(H_i)} \quad (1)$$

C.1 Forecasting metrics

Root Mean Square Error (RMSE)

$$\text{RMSE} = \frac{1}{N} \sum_{k=1}^N \sqrt{\frac{1}{H \times W} \sum_{i=1}^H \sum_{j=1}^W L(i) (\tilde{X}_{k,i,j} - X_{k,i,j})^2} \quad (2)$$

834 **Anomaly Correlation Coefficient (ACC)** is the spatial correlation between prediction anomalies
835 \tilde{X}' relative to climatology and ground truth anomalies X' relative to climatology:

$$\text{ACC} = \frac{\sum_{k,i,j} L(i) \tilde{X}'_{k,i,j} X'_{k,i,j}}{\sqrt{\sum_{k,i,j} L(i) \tilde{X}'_{k,i,j}{}^2 \sum_{k,i,j} L(i) X'_{k,i,j}{}^2}}, \quad (3)$$

$$\tilde{X}' = \tilde{X} - C, X' = X - C, \quad (4)$$

836 in which climatology C is the temporal mean of the ground truth data over a fixed period. We used
837 the climatology data from WeatherBench2 [76] in our all experiments.

838 **Spectral Divergence (SpecDiv)** is inspired by KL divergence, which computes the expectation of
839 the logarithmic ratio between the ground truth and predicted spectra. This metric emphasizes the
840 relative error between the frequency components of the ground truth and prediction:

$$\text{SpecDiv} = \sum_k S'(k) \cdot \log \left(\frac{S'(k)}{\tilde{S}'(k)} \right) \quad (5)$$

841 where $S'(k)$ and $\hat{S}'(k)$ represent the spectral components of the ground truth and predictions,
842 respectively, and k denotes the spectral component.

843 C.2 Climate downscaling and infilling metrics

844 **Root Mean Square Error (RMSE)** This is the same as Equation (2).

845 **Mean Bias** measures the mean difference between the prediction and the ground truth. A positive
846 mean bias shows overestimation, while a negative mean bias shows underestimation:

$$\text{Mean bias} = \frac{1}{N \times H \times W} \sum_{k=1}^N \sum_{i=1}^H \sum_{j=1}^W (\tilde{X}_{k,i,j} - X_{k,i,j}) \quad (6)$$

847 **Anomaly Pearson Coefficient** measures the Pearson correlation between the prediction and the
848 ground truth anomalies. We first flatten the prediction and ground truth anomalies, and compute the
849 metric as follows:

$$\rho_{\tilde{X}', X'} = \frac{\text{cov}(\tilde{X}', X')}{\sigma_{\tilde{X}'} \sigma_{X'}} \quad (7)$$

850 NOTE: For the Climate data infilling task, we compute the metrics over the masked cells only.

851 C.3 Climate model emulation metrics

852 **Normalized spatial root mean square error (NRMSE_s)** measures the spatial discrepancy between
853 the temporal mean of the prediction and the temporal mean of the ground truth:

$$\text{NRMSE}_s = \sqrt{\left\langle \left(\frac{1}{N} \sum_{k=1}^N \tilde{X} - \frac{1}{N} \sum_{k=1}^N X \right)^2 \right\rangle} / \frac{1}{N} \sum_{k=1}^N \langle X \rangle, \quad (8)$$

854 in which $\langle A \rangle$ is the global mean of A :

$$\langle A \rangle = \frac{1}{H \times W} \sum_{i=1}^H \sum_{j=1}^W L(i) A_{i,j} \quad (9)$$

855 **Normalized global root mean square error (NRMSE_g)** measures the discrepancy between the
856 global mean of the prediction and the global mean of the ground truth:

$$\text{NRMSE}_g = \sqrt{\frac{1}{N} \sum_{k=1}^N (\langle \tilde{X} \rangle - \langle X \rangle)^2} / \frac{1}{N} \sum_{k=1}^N \langle X \rangle. \quad (10)$$

857 **Total normalized root mean square error (Total)** is the weighted sum of NRMSE_s and NRMSE_g:

$$\text{Total} = \text{NRMSE}_s + \alpha \cdot \text{NRMSE}_g, \quad (11)$$

858 where α is chosen to be 5 as suggested by Watson-Parris et al. [97].

859 **C.4 Extreme weather events detection metrics**

860 Each pixel in the $H \times W$ grid is classified into one of three classes, leading to a confusion matrix per
 861 class (AR, TC, and BG). The performance metrics, calculated for each class, are defined as follows
 862 using the elements of the confusion matrix—True Positives (TP), False Positives (FP), True Negatives
 863 (TN), and False Negatives (FN):

864 **Intersection over Union (IoU)**

$$\text{IoU}_c = \frac{\text{TP}_c}{\text{TP}_c + \text{FP}_c + \text{FN}_c} \quad (12)$$

865 **Precision**

$$\text{Precision}_c = \frac{\text{TP}_c}{\text{TP}_c + \text{FP}_c} \quad (13)$$

866 **Recall**

$$\text{Recall}_c = \frac{\text{TP}_c}{\text{TP}_c + \text{FN}_c} \quad (14)$$

867 **F-1 Score**

$$\text{F-1}_c = 2 \times \frac{\text{Precision}_c \times \text{Recall}_c}{\text{Precision}_c + \text{Recall}_c} \quad (15)$$

868 **Specificity**

$$\text{Specificity}_c = \frac{\text{TN}_c}{\text{TN}_c + \text{FP}_c} \quad (16)$$

869 **D Experiment details**

870 This section details the experiments we conducted in Section 3, including model architectures and
 871 hyperparameters, training objectives, and optimization.

872 **D.1 Model architectures**

873 **Unet** We borrow our Unet implementation from PDEArena [29]. Table 7 shows hyperparameters of
 Unet we use in all our experiments. The Unet model has a total of 500M parameters.

Table 7: Default hyperparameters of UNet

Hyperparameter	Meaning	Value
Padding size	Padding size of each convolution layer	1
Kernel size	Kernel size of each convolution layer	3
Stride	Stride of each convolution layer	1
Channel multiplications	Determine the number of output channels for Down and Up blocks	[1, 2, 2, 4]
Blocks	Number of Resnet blocks	2
Use attention	If use attention in Down and Up blocks	False

874

875 **ClimaX and Stormer** For ClimaX and Stormer, we borrow the implementation from their original
 876 papers [59, 61], which we refer to for a detailed description of their architectures. Table 8 shows
 877 hyperparameters of ClimaX and Stormer we use in all our experiments. The parameter count for
 878 ClimaX and Stormer is 100M and 400M, respectively.

879 **D.1.1 Extensions for climate model emulation**

880 We modify the architecture of ClimaX and Stormer for this task to account for the time dimension T
 881 in the input. Each time slice of the input goes through the embedding layer and the transformer blocks
 882 independently, resulting in an output tensor of shape $T \times h \times w \times D$ where D is the embedding
 883 dimension. This tensor then goes through a global pooling layer along the spatial dimensions h and w ,

Table 8: Default hyperparameters of ClimaX and Stormer

Hyperparameter	Meaning	ClimaX	Stormer
p	Patch size	4	2
D	Embedding dimension	1024	1024
Depth	Number of ViT blocks	8	24
# heads	Number of attention heads	16	16
MLP ratio	Determine the hidden dimension of the MLP layer in a ViT block	4	4
Prediction depth	Number of layers of the prediction head	2	1
Hidden dimension	Hidden dimension of the prediction head	1024	N/A

884 outputting a tensor of shape $T \times D$. This sequence of tensors is aggregated by a cross-attention layer
 885 over the time dimension to a single vector of D dimensions. Finally, a linear layer predicts the output
 886 of shape $V \times H \times W$. The cross-attention layer along the time dimension is randomly initialized and
 887 trained together with the new embedding and prediction layer, as well as the transformer backbone.

888 D.1.2 Extensions for extreme weather events detection

889 Since the spatial resolution of ClimateNet is 768×1152 , training the original ClimaX and Stormer
 890 with patch sizes of 4 and 2, respectively, is too computationally expensive. To address this issue, we
 891 use a stack of 6 convolutional layers to embed the input before the attention blocks which outputs
 892 a tensor of shape $96 \times 144 \times D$, reducing the spatial resolution by 8. This tensor goes through the
 893 transformer blocks and a linear prediction head which outputs a tensor of shape $3 \times 96 \times 144$ where 3
 894 is the number of classes. Finally, this output is bilinearly interpolated to the original spatial resolution
 895 of 768×1152 . The bilinear interpolation module is also used by the baseline CGNet [103].

896 D.2 Training details

897 D.2.1 Data normalization

898 For tasks that utilize ERA5 for training and evaluation, including medium-range weather forecasting,
 899 S2S forecasting, climate downscaling, and climate data infilling, we normalize both input and output
 900 variables to have mean 0 and standard deviation 1. The normalization constants are computed across
 901 the entire training set. During evaluation, predictions and ground-truths are de-normalized to the
 902 original scale before computing the metrics.

903 For the extreme weather events detection task that uses ClimateNet, we normalize the input variables
 904 similarly to ERA5, but not the output variables since they are discrete labels.

905 For the climate model emulation task that uses ClimateBench, we normalize the input variables
 906 similarly to ERA5, but not the output variables since we predict each target variable separately.

907 D.2.2 Training objectives

908 **Regression** For the five regression tasks, including medium-range weather forecasting, S2S fore-
 909 casting, climate downscaling, climate data infilling, and climate model emulation, we use the same
 910 latitude-weighted mean-squared error loss for training:

$$\mathcal{L}(\theta) = \frac{1}{V' \times H \times W} \sum_{v=1}^{V'} \sum_{i=1}^H \sum_{j=1}^W L(i) (\tilde{X}^{v,i,j} - X^{v,i,j})^2. \quad (17)$$

911 **Classification** For the extreme weather events detection task, we utilize the weighted Jaccard loss
 912 proposed in Lacombe et al. [43] to prioritize the TC and AR classes:

$$\mathcal{L}(\theta) = \frac{1}{C \times H \times W} \sum_{c=1}^C \sum_{i=1}^H \sum_{j=1}^W \left(1 - w_c \frac{\tilde{X}^{c,i,j} X^{c,i,j}}{(\tilde{X}^{c,i,j} + X^{c,i,j}) - \tilde{X}^{c,i,j} X^{c,i,j}} \right), \quad (18)$$

913 in which w_c is the weight of class c . Following Lacombe et al. [43], we set w_c to 0.678, 31.08, and
 914 2.9 for BG, TC, and AR, respectively.

915 **D.2.3 Optimization**

916 For all tasks, we used AdamW with parameters ($\beta_1 = 0.9, \beta_2 = 0.95$) and weight decay of $1e - 5$ for
917 all parameters except for the positional embedding in ClimaX and Stormer. We trained each model
918 for 50 epochs with a batch size of 32, using a linear warmup schedule for 5 epochs, followed by a
cosine-annealing schedule for 45 epochs. Table 9 shows the peak learning rate for each task.

Table 9: Learning rate for finetuning ClimaX in different downstream tasks

Task	Finetuning LR	Scratch Training LR
Medium-range weather forecasting	$5e - 6$	$5e - 4$
S2S forecasting	$5e - 5$	$5e - 4$
Climate downscaling	$5e - 5$	$5e - 4$
Climate data infilling	$1e - 4$	$5e - 4$
Climate model emulation	$5e - 4$	$5e - 4$
Extreme weather events detection	$5e - 4$	$5e - 4$

919

920 For finetuning ClimaX and Stormer, we used a smaller learning rate for tasks that are similar to
921 pretraining and a larger learning rate for tasks that are more different.

922 **D.2.4 Software and hardware stack**

923 We use PyTorch [62], numpy [32] and xarray [36] to manage our data and model training. We also
924 use `timm` [102] for implementations of ClimaX and Stormer. All training is done on 8 NVIDIA RTX
925 A6000 GPUs. We leverage fp16 floating point precision in our experiments.

926 **E Visualizations**

927 **E.1 S2S forecasting**

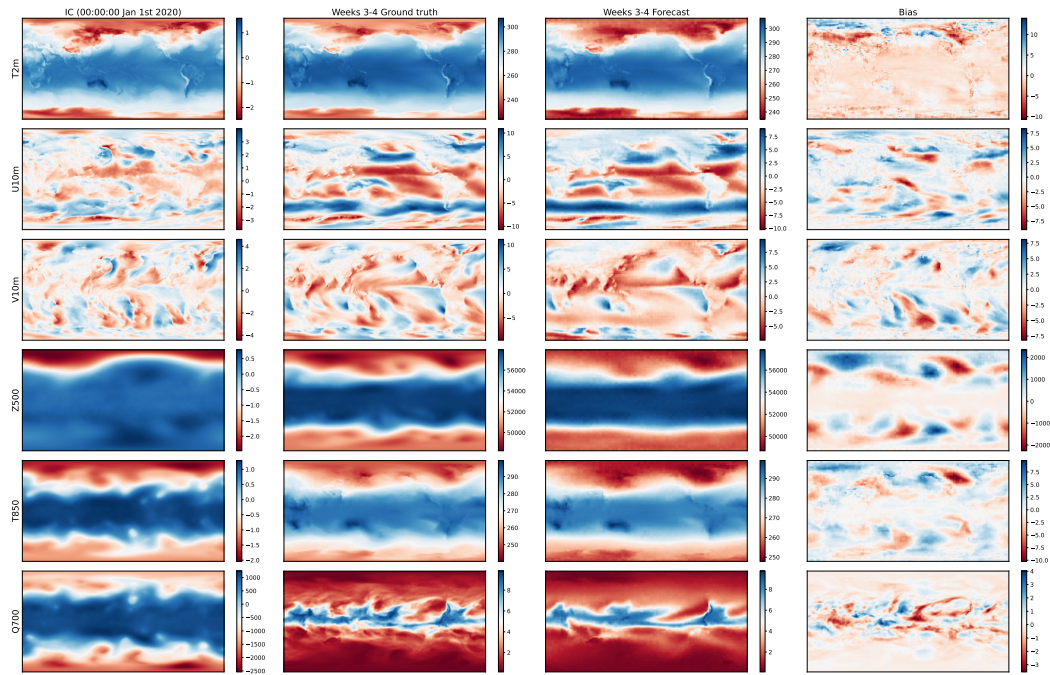


Figure 4: ClimaX forecasts for weeks 3-4 of six target variables.

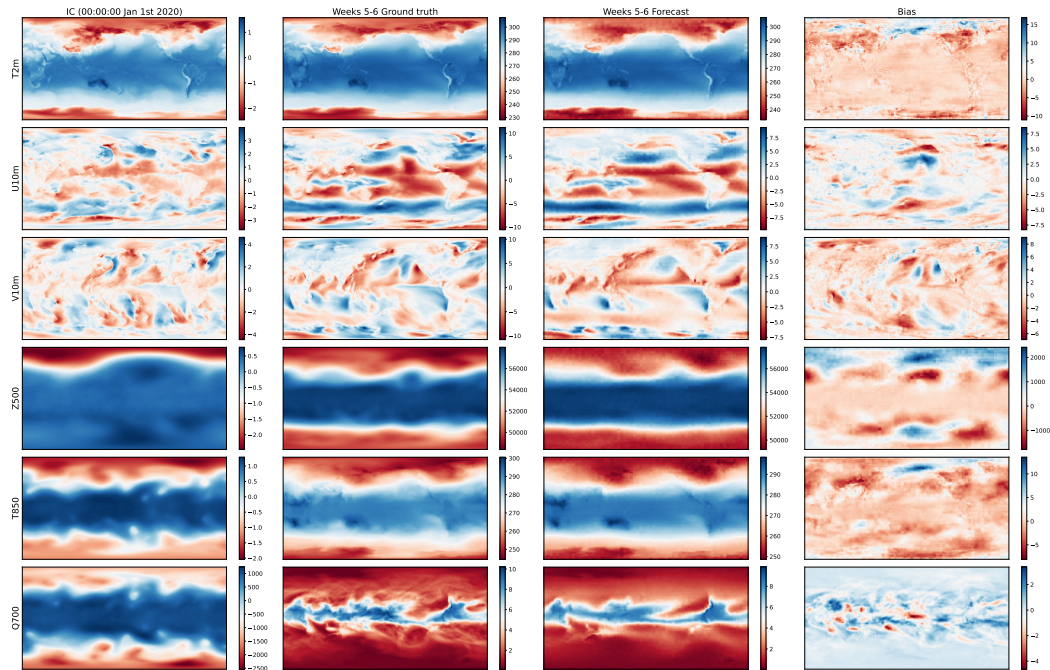


Figure 5: ClimaX forecasts for weeks 5-6 of six target variables.

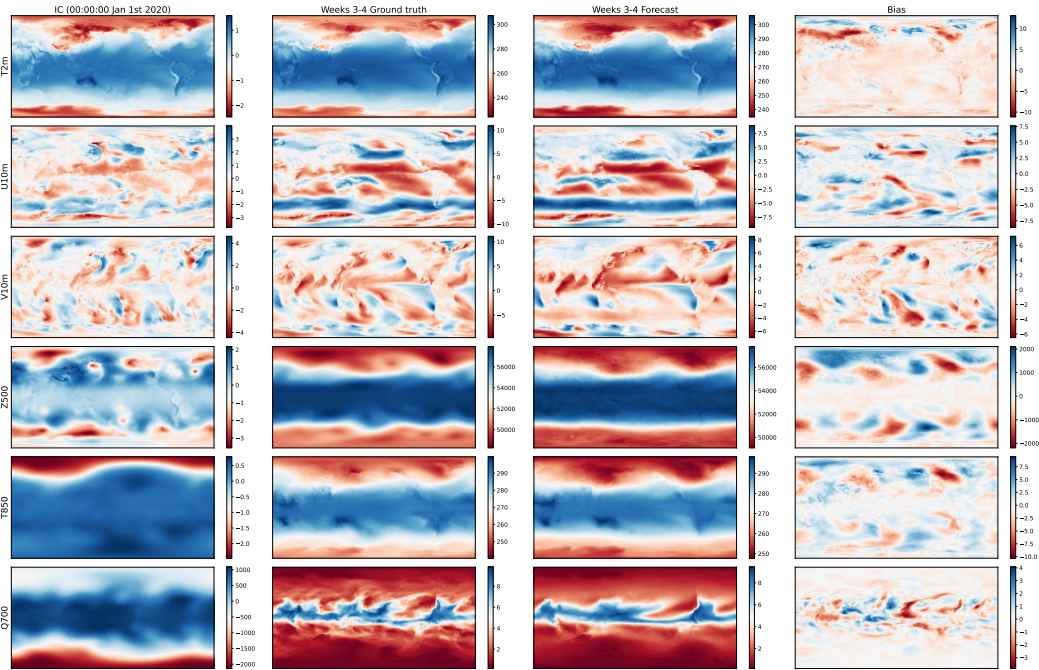


Figure 6: Stormer forecasts for weeks 3-4 of six target variables.

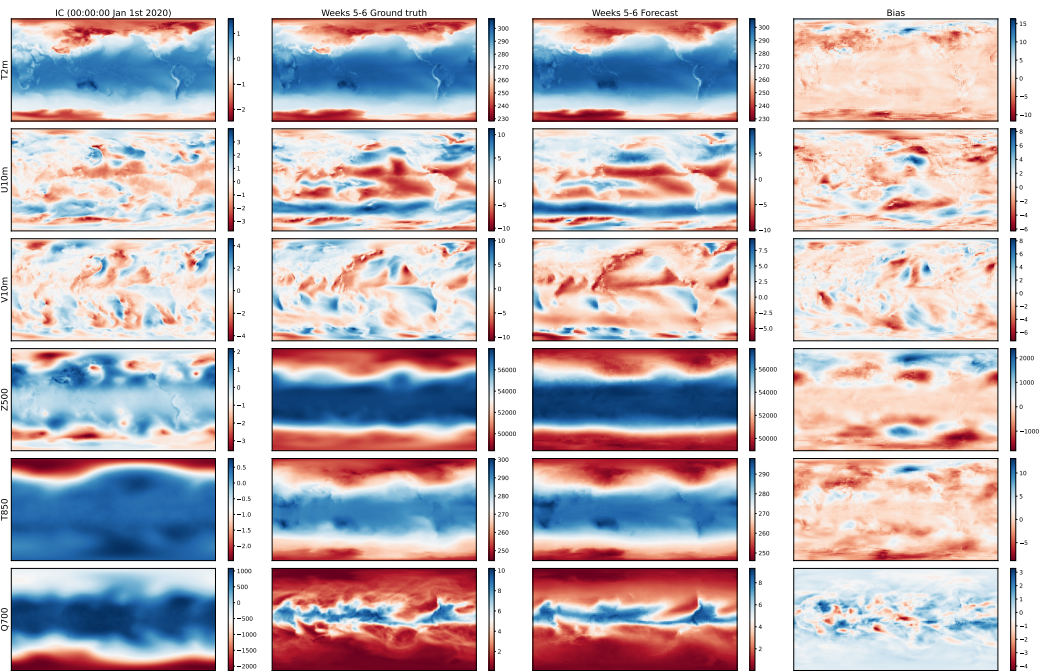


Figure 7: Stormer forecasts for weeks 5-6 of six target variables.

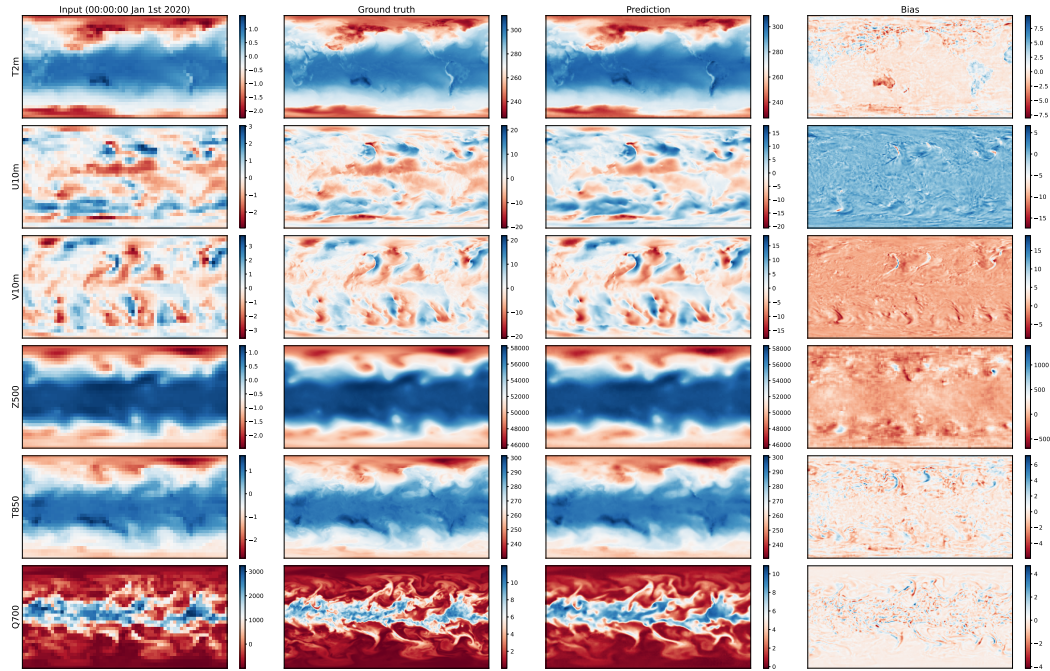


Figure 8: ClimaX downscaling predictions of six target variables.

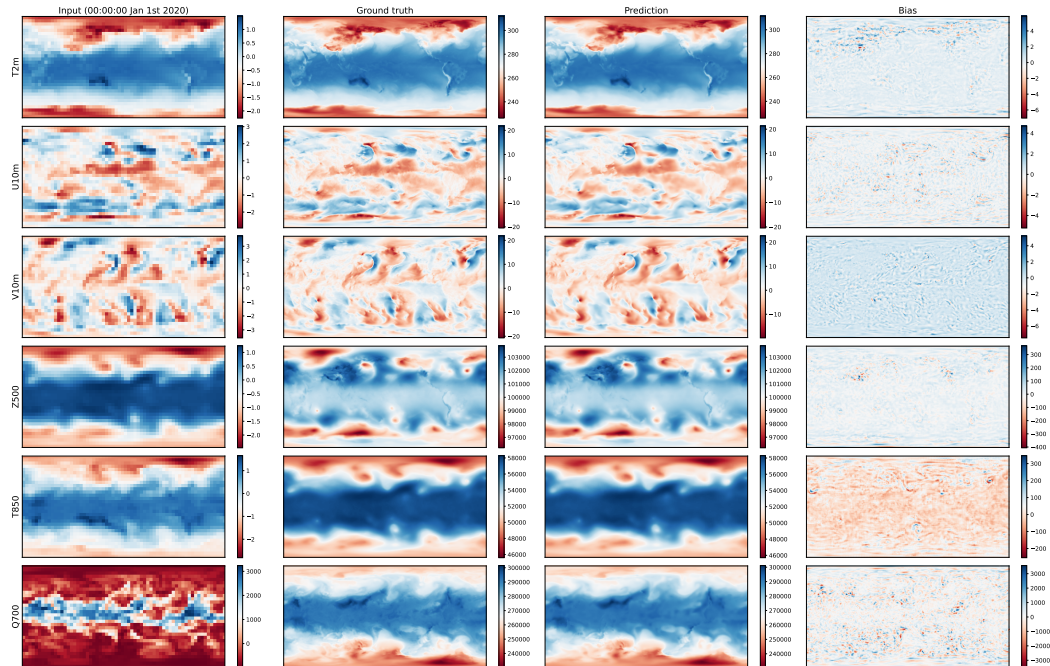


Figure 9: Stormer downscaling predictions of six target variables.

929 **F Atmospheric chemistry**

930 This section presents the atmospheric chemistry tasks that AtmosArena includes.

931 **F.1 Atmospheric chemistry downscaling**

932 Atmospheric chemistry simulations are essential for understanding various global processes such as air
933 pollution, biogeochemical cycles, and climate change. High-resolution models can capture fine-scale
934 chemical interactions, providing insights into local pollution levels and their health impacts. However,
935 these models are computationally intensive. Deep learning offers a solution by transforming coarse-
936 resolution inputs into finer-resolution outputs [27]. Specifically, the input is a grid of dimensions
937 $V \times H \times W$, and the output is a higher-resolution grid $V' \times H' \times W'$, where $H' > H$ and $W' > W$.
938 This allows for precise monitoring of atmospheric pollutants and their effects on human health and
939 the environment, enabling more informed policy decisions and scientific research.

940 **Dataset** We utilize GEOS-CF, a simulated dataset from the NASA GEOS Composition Forecast
941 (GEOS-CF) system [40]. GEOS-CF combines the NASA GEOS model with the GEOS-Chem
942 chemical transport model to simulate the atmospheric composition [39]. The dataset offers outputs
943 on a 0.25° grid, which we downsample to 5.625° for the low-resolution input and 1.40625° for the
944 high-resolution output. For our benchmark, we use the meteorological replay simulation (“das” files),
945 covering the years 2018 to the present. We focus on downscaling the five near-surface atmospheric
946 pollutants: NO₂, SO₂, CO, O₃, and PM_{2.5}, averaged over a 1-hour window (“chm_tavg_1hr” files).

947 **F.2 Atmospheric composition forecasting**

948 This task involves predicting the global atmospheric composition of important air pollutants such as
949 carbon monoxide and carbon dioxide at different lead times. This task is crucial for understanding air
950 quality, which directly impacts human health by influencing the prevalence of non-communicable
951 diseases. This task presents a significant challenge to data-driven models due to the complexity of
952 atmospheric dynamics and the influence of human activities on emission levels. The task formulation
953 and input and output shapes are similar to weather forecasting.

954 **Dataset** We use CAMS Analysis maintained by ECMWF for the atmospheric composition forecasting
955 task in AtmosArena. As part of the Copernicus Atmosphere Monitoring Service (CAMS), this dataset
956 integrates meteorological variables with concentrations of air pollutants such as carbon monoxide and
957 carbon dioxide, providing a comprehensive overview of global atmospheric composition. The dataset
958 offers 12-hourly data at a 0.4° (450×900 grids) resolution from 2017 to the present. Similar to
959 ERA5, we regrid this dataset to the common resolution of 1.40625° for easier training and evaluation.

960 **G Additional experiments**

961 **G.1 Atmospheric chemistry experiments**

962 **G.1.1 Atmospheric chemistry downscaling**

963 We consider the task of downscaling for five near-surface variables: NO₂, SO₂, CO, O₃, and
964 PM_{2.5}. We use GEOS-CF at 5.625° as the low-resolution input, and GEOS-CF at 1.40625° as the
965 high-resolution target, corresponding to $4\times$ upsampling. We use 2018-2020 for training, 2021 for
966 validation, and 2020 for testing. Due to time and compute constraints, we only consider ClimaX
finetuned and Unet as baselines.

Table 10: MAE of ClimaX finetuned and Unet for downscaling five target near-surface pollutants.

	NO ₂	SO ₂	CO	O ₃	PM _{2.5}
ClimaX finetuned	0.069	0.049	0.405	0.0065	0.100
Unet	0.064	0.047		0.0071	0.104

967

968 Table 10 reports the MAE metric in the log space of the five target variables. ClimaX finetuned and
 969 Unet perform competitively. Given the results in climate downscaling, we believe fully finetuned
 970 Stormer will outperform Unet in this task.

971 G.1.2 Atmospheric composition forecasting

972 We compare ClimaX with Unet on forecasting eight near-surface pollutants: Total Column Carbon
 973 Monoxide (TC CO), Total Column Nitric Oxide (TC NO), Total Column Nitrogen Dioxide (TC
 974 NO₂), Total Column Sulfur Dioxide (TC SO₂), Total Column Ozone (TC O₃), Particulate Matter
 975 1um (PM₁), Particulate Matter 2.5um (PM_{2.5}), and Particulate Matter 10um (PM₁₀), with lead times
 976 from 1 to 3 days. For each baseline method, we finetune a separate model for each specific lead time
 977 and target variable. We use CAMS Analysis from 2017 to 2020 for training, 2021 for validation, and
 2022 for testing.

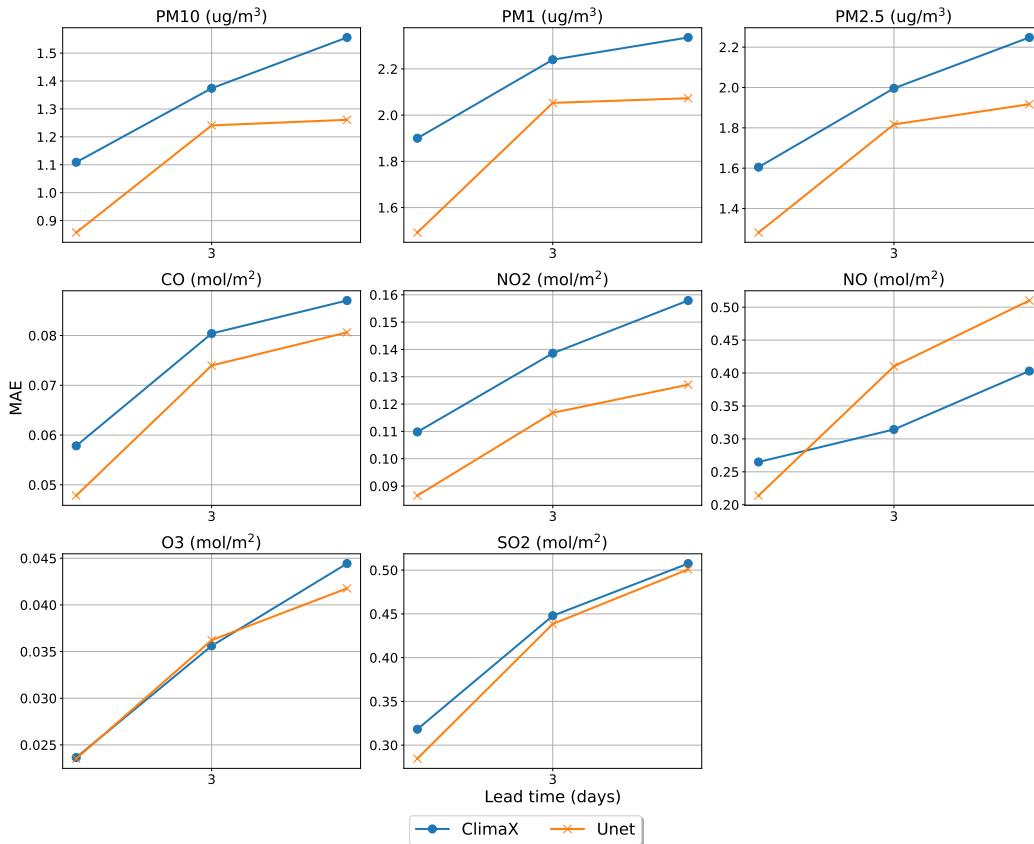


Figure 10: Air composition forecasting performance.

978

979 Figure 10 shows the performance of ClimaX and Unet on forecasting eight key pollutants from 1 day
 980 to 5 days. Unet outperforms ClimaX for almost all variables. This result shows that the temporal
 981 forecasting capabilities of pretrained models may not transfer well to new tasks in a new domain.

982 G.2 Additional metrics for atmospheric physics tasks

983 **S2S forecasting** In addition to RMSE and ACC, we report Spectral Divergence as a physics-based
 984 metric, which measures the discrepancy between the frequency components of the ground truth and
 985 prediction. Table 11 shows the superior performance of ClimaX frozen across all variables and lead
 986 times. This highlights the effectiveness of multi-source pretraining in obtaining a general-purpose
 987 backbone that can adapt to forecasting tasks with unseen time scales only via lightweight finetuning.

Table 11: S2S performance measured by Spectral Div on four target variables at two lead times.

		Z500		T850		T2m		Q700	
		Weeks 3-4	Weeks 5-6	Weeks 3-4	Weeks 5-6	Weeks 3-4	Weeks 5-6	Weeks 3-4	Weeks 5-6
		Spectral Div (↓)	ClimaX frozen	0	0	0.3153	0.2894	0.1671	0.1805
	ClimaX finetuned	0	0	0.3224	0.3180	0.2298	0.2093	0.0930	0.0937
	Stormer frozen	0	0	0.3307	0.4161	0.4705	0.5971	0.5188	0.7513
	Stormer finetuned	0	0	0.3275	0.3024	0.6603	0.6105	0.4337	0.3468
	Unet	0	0	0.3863	0.5110	0.2065	0.4647	0.0809	0.8157

988 **Downscaling** Table 12 shows the Anomaly Pearson Coefficient of different baselines on the climate
 989 downscaling tasks. Stormer finetuned is the best method for all four variables. However, all baselines
 990 achieve very similar performances, suggesting Anomaly Pearson Coefficient may not be the best
 metric for distinguishing different models in this task. A similar result was observed in ClimaX [59].

Table 12: Downscaling performance measured by Anomaly Pearson Coefficient on six variables.

		Z500	T850	T2m	Q700	U10	V10
		Anomaly Pearson (↑)	ClimaX frozen	0.9963	0.9879	0.9833	0.9388
	ClimaX finetuned	0.9977	0.9907	0.9869	0.9532	0.9802	0.9813
	Stormer frozen	0.9956	0.9856	0.9821	0.9240	0.9654	0.9689
	Stormer finetuned	0.9993	0.9951	0.9946	0.9626	0.9886	0.9894
	Unet	0.9987	0.9931	0.9917	0.9613	0.9850	0.9861

991

992 **Extreme weather events detection** Table 13 shows the Specificity metrics of different methods in
 993 the extreme weather events detection tasks. ClimaX frozen is the best-performing method, showing
 994 the effectiveness of multi-source pretraining in transferring the backbone to a completely new task.
 995 However, the baselines perform very similarly for this metric, suggesting it may not be the best to
 evaluate methods in this task.

Table 13: Specificity Metrics of different methods for TC and AR detection.

	ClimaX frozen	ClimaX finetuned	Stormer frozen	Stormer finetuned	CGNet
TC	0.99	0.99	0.98	0.98	0.99
AR	0.96	0.96	0.95	0.95	0.92

996

997 G.3 Climate data infilling on Berkeley Earth

998 We test the models trained to perform infilling for ERA5 in Sections 4.4 on the Berkeley Earth dataset
 999 to examine their transferability between datasets. Similarly to ERA5, we generate a fixed set of masks
 1000 during testing, with the mask ratio $r \in \{0.1, 0.3, 0.5, 0.7, 0.9\}$. We test the models on infilling for
 1001 data from 2020 to 2023. Figure 11 shows that all methods perform similarly for this dataset, and the
 1002 performances do not get worse as we increase the mask ratio. We hypothesize that because of the
 1003 distribution shift from ERA5 to Berkeley Earth, the best thing the models can do is to predict the
 1004 average, leading to very similar performances among models and mask ratios.

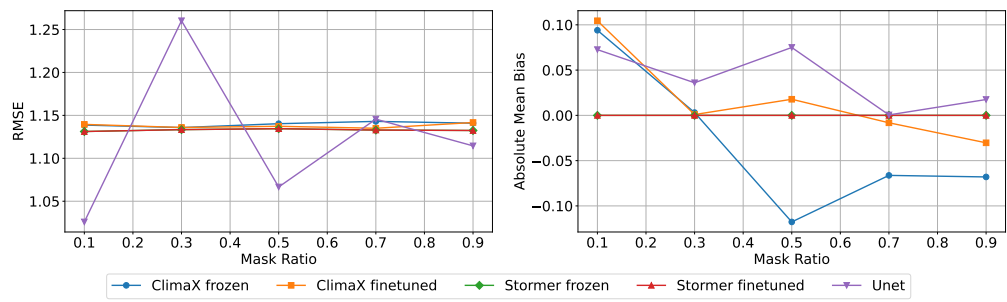


Figure 11: Performance of different models measured by RMSE and Absolute Mean Bias on infilling the Berkeley Earth temperature data with different mask ratios.